NSG-7530

CLOUDS ABOVE THE MARTIAN LIMB: VIKING OBSERVATIONS

Leonard J. Martin, William A. Baum, Lawrence H. Wasserman, and Tobias J. Kreidl

Planetary Research Center, Lowell Observatory,

Flagstaff, Arizona 86002

Manuscript totals 65 pages, with one table and 27 figures.

RUNNING PAGE HEAD: MARTIAN LIMB CLOUD OBSERVATIONS

SEND PROOFS TO: Leonard J. Martin
Lowell Observatory
Post Office Box 1269
Flagstaff, Arizona 86002

ABSTRACT

Whenever Viking Orbiter images included the limb of Mars, they recorded one or more layers of clouds above the limb. The height above the limb and the brightness (reflectivity) of these clouds have been determined in a selected group of these images. Despite a number of constraints, we attempted to find suitable images representing different seasons, phase angles, latitudes, longitudes, and filter colors. This paper represents the results obtained from 57 Viking Orbiter images. Graphs of the results illustrate the possible influence of various parameters.

We show normalized individual brightness profiles of three separate traverses across the limb of each image. The most notable finding is that some of these clouds can be very high. Many reach heights of over 60 km, and several are over 70 km above the limb. Statistically, the reflectivity of the clouds increases with phase angle. Reflectivity and height both appear to vary with season, but the selected images spanned only one Martian year, so the role of seasons cannot be isolated. Limb clouds in red-filter images tend to be brighter than violet-filter images, but both season and phase appear to be more dominant factors. Due to the limited sample available, the possible influences of latitude and longitude are less clear. The layering of these clouds ranges from a single layer to five or more layers. Reflectivity gradients range from smooth and gentle to

steep and irregular. This study provides further evidence for a changeable and complex Martian atmosphere.

INTRODUCTION

Clouds on Mars have been observed for over a century using Earthbound telescopes. Dust storms, polar hoods, seasonal clouds, diurnal clouds, reoccurring clouds, cloud motions, hazes, dark clouds, and clouds visible only through blue or violet filters have been well known and studied long before the earliest spacecraft flew by Mars (Slipher, 1962; Capen, 1972). The primary purpose in Percival Lowell's founding of his observatory was to study Mars; and in 1969, when the International Planetary Patrol was established at Lowell Observatory (Baum et al., 1970), the primary purpose was to intensively photograph Mars and thereby to increase our knowledge of these atmospheric phenomena. By establishing a network of observatories around our globe, we were able to monitor Martian clouds continuously on a nearly hourly basis. Mariner 9 and the Viking Orbiters not only confirmed these Earth-based observations but resolved many smaller and fainter clouds (Briggs et al., 1977; French et al., 1981). Most of the brightenings on Earth-based photographs that we had thought might be clouds were indeed clouds (Martin, 1983). Mars is generally much cloudier than most astronomers had previously suspected.

The Viking Orbiters took a number of pictures of the Martian limb and therefore provided an opportunity to investigate the vertical distribution of clouds by observing them edge-on. More precisely, of course, we are viewing an overlaid stack of spherical shells in the Martian atmosphere, so the edge-on brightness at the limb does not directly represent the vertical distribution of scattering particles. To obtain the latter, one must adopt a scattering theory (for example, Lumme et al., 1981a), make assumptions about the horizontal uniformity of cloud layers, and perform an "inversion" of the observed edge-on limb brightness profiles. The theory and the inversions are not dealt with in the present paper.

There were several limitations in the data sample available. Only a very small percentage of frames taken by the two orbiters included the limb, and such frames were scheduled only sporadically during the mission. Moreover, many of the limb pictures were not usable for this study because the position of the limb could not be determined, the phase angle was too low, or the clouds were overexposed.

One of the main tasks in this study was to find out where the surface limbs are, so that the heights of cloud layers could be specified on a scale with a known zero point. In all limb frames the surface limb is obscured by clouds or haze, and in most of the frames a visual estimate of the surface limb locus could easily go wrong by 10 or 20 km. The method we chose for locating the surface limb beneath

the cloud blanket was based on measuring the positions of a number of foreground craters that were identifiable members of the control net established by Davies et al. (1978). This choice systematically excluded the use of images over the polar caps. It also excluded images taken over areas where the control net was sparse and those in which the control net craters were too small to be identifiable on the image. And, of course, images could not be used if the clouds were too dense for foreground craters to be visible.

Measuring crater positions required specially processed images that were geometrically corrected, and the limb traverses were derived from special-order computer tapes of geometrically corrected images purchased from the Jet Propulsion Laboratory. The cost of these tapes limited the number of images we were able to select.

Because of the problems cited above, our data set is not ideal. It was not possible to sample all combinations of phase angle, season, latitude, longitude, and filter color. Nevertheless, the 57 images that were successfully measured provide a wealth of information about the Martian atmosphere.

PROCEDURES

Locating the Limb

Calculating the precise locus of the obscured surface limb on each of the selected images began with the identification of control net craters (Davies et al., 1978; Davies, 1981, 1982) on Jet Propulsion Laboratory (JPL) Viking photographs. The centerpoint of each identifiable control net crater was then measured on geometrically corrected versions of those images. Those measurements were made either on gridded photographs (hard copy) or, in some cases, on our Grinnell image processor using magnetic tapes of the images to input to our DEC PDP-11/55 computer. The gridded photographs and the magnetic tapes of geometrically corrected images were both furnished by JPL. Using either method, the measuring proved to be accurate but tedious.

Figure 1

A computer program was developed to calculate the limb locus by matching our crater position measurements with the longitudes and latitudes assigned to them by Davies. We adopted the SEDR height of the spacecraft at the moment of exposure and an assumed radius for Mars (3385 km), while permitting other SEDR parameters, such as the longitude and latitude of the sub-spacecraft point, to float.

This computer program was extensively tested and refined by using it on an image (profile set no. 20) that was relatively cloud-free and whose surface limb locus could be visually estimated quite closely on

the gridded photograph. The computer program and its underlying assumptions evolved through a series of trial variations whose relative merits were judged by comparing the computed limb to that seen on the test image.

In each image, before doing a least-squares fit to the control-net craters, a preliminary check was performed on the data. The pixel distance from each crater to every other crater was calculated and compared with the control-net values. If a crater was strongly discordant with the rest, it was rejected.

Some of the selected images had more than 40 usable control craters, while two images had as few as nine. Of course, the accuracy of the limb is higher for images having a larger number of well-distributed control net craters. Data from images that include large changes in elevation may be affected by factors that are not taken into account by the program. Nevertheless, we believe that the maximum error in the limb locus is no more than 5 km for any image and that the average error is probably less than 2 km. The profiles of the limb traverses (Figures 12-27) appear to confirm this level of accuracy.

Profiles Across the Limb

The Lowell computer, image processor, and plotter were used to construct the profiles in Figures 12-27. These were derived from

magnetic tapes of the Viking Orbiter images that had been specially processed at JPL to include shading correction and geometric correction but were otherwise raw copies of the originals. Unlike the photographic prints used for measuring craters, they did not include high pass filtering or gridding.

In each image, three traverses were made perpendicular to the limb, extending from empty sky background to points well inside the limb. These three traverses were typically on the order of 100 km apart at the limb. (Five traverses were made on image 37.) Raw profiles were constructed using interpolated pixel values along the traverse. These raw profiles were then brought to common scales in both dimensions. The horizontal scale is in kilometers up from the limb based upon the image scale at the limb for each image. The vertical scale is reflectance calculated from the solar constant, filter factors, exposure times, gain settings, vidicon calibrations, and distances from the Sun.

Aboard the Viking orbiters, the output signal of each of the vidicon camera systems was approximately linear with light input, but there was a bias level (or "pedestal") such that the output was roughly 20 of full scale at zero light input. Ordinarily, an "offset" was subtracted from the signal with the intention of canceling this pedestal before the output was transmitted to the Earth. But drifts in the electronics resulted in a slight over-subtraction during most of

the mission, causing low light levels to be clipped and irretrievably lost. To avoid losing faint limb clouds, most limb frames were obtained with a special uplinking command that inhibited the offset and permitted the full signal to be transmitted. Thus, most of our limb profiles are valid all the way out to the faintest limb clouds. Within our data set, there are six cases (namely, images 24-28, and 47) when the offset was not inhibited. For them, the peak reflectivities quoted in Table I may be slightly too low and the heights of the highest clouds may be substantially underestimated.

Table I

The values given in Table I for maximum reflectance and for latitude and longitude of the limb were generated by the computer, whereas the heights of the highest clouds were determined by visual inspection of the profiles. When high, thin cloud layers were close to the noise level of the sky, their reality was checked by inspection of contrast-enhanced images on the Grinnell display monitor.

Observations

In Table I the images are listed and numbered in chronological order but divided into two sets so that Viking Orbiter 1 images are listed first (1-37), followed by Viking Orbiter 2 (38-57). The letters "A" and "B" in the Viking Picno (picture numbers) indicate which spacecraft (1 or 2) took the picture. The first three digits of this

number refer to the revolution number of the spacecraft, while the last two digits are frame numbers within that orbit, in chronological order. Martian season is indicated by L_s, which is the areocentric longitude of the Sun measured eastward from its vernal equinox. This parameter is also the horizontal scale in Figures 3 and 4.

The individual profiles within each frame are designated "a," "b," and "c." Although the order was arbitrary, profile "b" is generally the middle one, and it was always used to generate the plots for Figures 4-11. In cases where two or more pictures covered the same area, no attempt was made to cross the limb at the same points on profiles from those images. The profiles appear in figures 12-27, but the numerical order was modified to try to minimize the number of figures and to group similar cases. In the case of seasonal group C (defined in Figure 3), the red-filter images are on one figure, while the violet are on another.

Figures 2-11

RESULTS

Correlations

Figures 2-11 consist of one map and ten diagrams showing where correlations may or may not exist among various parameters associated with the 57 selected images. Within the limitations of the sample, we compare latitude, longitude, season, phase angle, filter color,

reflectivity of the limb clouds and their maximum heights. Some of these diagrams suggest relationships, whereas others suggest that no conclusions can be drawn. Our comments are in the captions.

Seasonal Groupings (Figure 3)

Group A is mid-fall in the southern hemisphere. It is represented by images 32-36 (Figure 21). These five images have very low phase angles, which probably account for their low reflectances. Images 32 and 33 have the lowest phase angles in this study. Other parameters such as season and areographic location were less significant. Clouds beyond the limb that show on limb frames having larger phase angles would have been in darkness on these pictures since the terminator was just beyond the limb.

Group B includes images 1-30 plus 37, which span L_s $85° \leq L_s \leq 135°$. This was from the end of northern spring to the middle of northern summer on Mars. Viking infrared thermal data showed that the Martian atmosphere was relatively free of dust during this period (Martin, 1981b). Images 1-12 have limbs between 30° and 50° north, whereas the remainder of the group is in the southern hemisphere. The images in Group B were taken from Viking Orbiter 1. Red frames obtained during this Martian season tended on average to yield higher reflectivity values than violet frames. Profile 37d includes the

highest clouds sampled with in Seasonal Group B.

Group C is in early northern-fall and prior to the onset of both planet-encircling dust storms. Images 38-45 include three red-filter frames (Figure 22) and five violet-filter frames (Figure 23). These are the earliest pictures selected from Viking Orbiter 2. As a group, they span less than three weeks' time, and all have phase angles between 71° and 79°. Furthermore, they all face to the west of north, although to varying degrees. Both the red and violet images selected for this season can be characterized as having great cloud heights (from 60 to over 70 km). The violet images have low reflectances, whereas the red-filter images have moderate reflectances (Figure 4). The red-filter images from Seasonal Group C are widely separated in longitude, although only 10° apart in latitude (Figure 2). All have high multilayered clouds above a heavily obscured limb.

Group D is in southern summer, following the two planet-encircling dust storms of 1977 (Briggs et al., 1979). The locations of images 46-57 are scattered throughout the southern hemisphere (Figure 2). They were taken through red filters; and, except for no. 31, were from Viking Orbiter 2. All except nos. 47 and 31 have high reflectances. The images in this group fall into one of two subgroups based upon the height of their limb clouds (Figure 4). Four of the five in the subgroup of lower heights have limbs at areocentric longitudes between 55° and 90°, whereas the other "D's" are outside

this range. (No. 31 is the exception, perhaps because of its low phase angle and/or because, unlike the others, it faces west.) In the final six images, the image to the south is the more distinctly layered member of each pair. Nos. 56 and 57 have the highest cloud reflectivity in their seasonal group.

Individual Profiles

Much of the resulting information may be gleaned from the brightness profiles of clouds in individual images and is not dependent on statistics based on incomplete sampling. For this reason, an appendix has been included, consisting of notes on many of the profiles that are plotted in Figures 12 through 27. These notes have been written to avoid repetition and to use individual profiles as examples of phenomena that often apply to other cases as well. Theoretical interpretation (Lumme et al., 1981b) of the profiles has been dealt with separately.

Figures 12-27

SUMMARY

Clouds on Mars were commonly found up to maximum heights between 35 and 70 km above the limb. Leovy et al. (1972) found cloud layers nearly this high using Mariner 9 data, but during the 1971 dust storm.

French and Taylor (1981) found evidence for inversion layers at similar altitudes from data derived from the occultation of ε Geminorum by Mars. Snyder (1979) reported that Barnes had found some clouds to be 80 km high, based upon shadow measurements. Some time periods seem more likely to have higher clouds than others. These periods may denote seasonal changes, but our sample was not comprehensive enough to determine that. Maximum cloud heights appear to correlate with latitude and longitude, but we are unable to say how repeatable that correlation might be at other times. A study by French et al. (1981) compared cloud locations found by Mariner 9 and by Viking during similar seasons of different Martian years Although the sampling was uneven in both cases, their maps seem to show a difference between years that is greater than seasonal differences. Extremely low phase angles probably also have an effect on apparent cloud detectability and therefore on apparent maximum cloud height.

The reflectances of limb clouds also vary with time and possibly season. Phase angles, however, appear to be the predominant variable, especially on violet-filter images. The relationship between reflectances and heights of limb clouds also changes with time and probably with other variables, as well. In most cases, the reflectances decreased as the profiles crossed above the limb; however, exceptions are seen on figure no. 15.

The profiles of individual images and groups of images are

informative, showing a wide variation in cloud structure and complexity. The color comparisons demonstrate that the composition of the clouds is not homogeneous: color differences have been commonly used to determine which clouds are dust and which are condensates (Huguenin and Clifford, 1982). Although it may still be impossible to determine how much is dust, how much is water, and how much is CO_2, the photometric properties of these clouds can be used for theoretical interpretation (Baum et al., 1977; Lumme et al., 1981). Non-limb Viking pictures and Earth-based photography also show differences when clouds are imaged through different colored filters, so that such differences are not unexpected on the limb pictures (Briggs et al., 1979; Capen, 1972; Martin, 1976, 1981a). They merely added a new dimension to these differences.

ACKNOWLEDGMENTS

We wish to thank the Jet Propulsion Laboratory, which provided the Viking materials necessary for this project. JPL employees who gave us particular help in obtaining the material were Sue LaVoie, Gordon Johnston, Nancy Evans (now at NASA Headquarters), and John Wellman, who helped in the initial planning and image selection for the project. In addition, we thank Hermann F. Haupt of the Institut für Astronomie der Universität Graz, who did some of the tedious

crater measuring. H. F. Haupt is obliged to Österreichische Forschungsgemeinschaft for a travel grant that made this cooperation possible. Merton L. Davies of Rand Corporation was most helpful in providing updates to his Mars control net data. We also thank Stuart E. Jones of Lowell Observatory for his photo lab work and Helen Horstman, who prepared the manuscript. Funding was provided under NASA Research Grant NSG-7530 (Mars Data Analysis Program). Additional funding was provided by Lowell Observatory, thanks to our Sole Trustee Michael C. J. Putnam.

REFERENCES

Baum, W. A., L. J. Martin, L. H. Wasserman, J. B. Wellman, and S. Eberle. (1977). The vertical distribution of scattering particles in the Martian atmosphere. Bull. Amer. Astron. Soc. 9, 514.

Baum, W. A., R. L. Millis, S. E. Jones, S. E., and L. J. Martin. (1970). The International Planetary Patrol Program. Icarus 12, 435-439.

Briggs, G. A., W. A. Baum, and J. Barres. (1979). Viking orbiter imaging observations of dust in the Martian atmosphere. J. Geophys. Res. 84, 2795-2820.

Briggs, G. A., K. Klaasen, T. Thorpe, J. Wellman, and W. Baum. (1977). Martian dynamic phenomena during June-November 1976: Viking

orbiter imaging results. J. Geophys. Res. 82, 4121-4149.

Capen, C. F. (1972). Contributions to sections 3.5, 3.6, 4.0, 4.1, and 4.2 of Mars Scientific Model (C. Michaux and R. L. Newburn, Eds.). JPL Document No. 606-1. Jet Propulsion Laboratory, Pasadena.

Davies, M. E. (1981, 1982). Personal communications.

Davies, M. E., F. Y. Katayama, and J. A. Roth. (1978). Control Net of Mars: February 1978, R-2309-NASA. The Rand Corporation, Santa Monica.

French, R. G., P. J. Gierasch, B. D. Popp, and R. J. Verdon. (1981). Global patterns in cloud forms on Mars. Icarus 45, 468-493.

French, R. G., and G. E. Taylor (1981). Occultation of ε Geminorum by Mars. IV. Oblateness of the Martian upper atmosphere. Icarus 45, 577-585.

Huguenin, R. L., and S. M. Clifford. (1982). Remote sensing evidence for regolith water vapor sources on Mars. J. Geophys. Res. 87, 10227-10251.

Inge, J. L. (1973). Martian albedo features and topography. Mercator map (1:25,000,000). Lowell Obs. Map Series. Also Mercury 2 (No. 6), 10 (centerfold).

Leovy, C. B., G. A. Briggs, A. T. Young, B. A. Smith, J. P. Pollack, E. N. Shipley, and R. L. Wildey. (1972). The Martian atmosphere: Mariner 9 television experiment progress report. Icarus 17, 373-393.

Lumme, K., L. J. Martin, and W. A. Baum. (1981a). Theoretical interpretation of photometric properties of the Martian surface and atmosphere. Icarus 45, 379-397.

Lumme, K., L. J. Martin, L. H. Wasserman, and W. A. Baum. (1981b). Theoretical interpretation of the Martian limb brightness profile. Bull. Amer. Astron. Soc. 13, 712.

Martin, L. J. (1974). The major Martian yellow storm of 1971. Icarus 22, 175-188.

Martin, L. J. (1976). 1973 dust storm on Mars: Maps from hourly photographs. Icarus 29, 363-380.

Martin, L. J. (1981a). A closer look at a developing Martian dust storm: Analysis of Viking images. Bull. Amer. Astron. Soc. 13, 708.

Martin, L. J. (1983). Mars from Earth and space. Sky and Telescope 65, 559.

Martin, T. Z. (1981b). Mean thermal and albedo behavior of the Mars surface and atmosphere over a Martian year. Icarus 45, 427-446.

Slipher, E. C. (1962). Mars--The Photographic Story. Northland Press, Flagstaff, Arizona.

Snyder, C. W. (1979). The planet Mars as seen at the end of the Viking mission. J. Geophys. Res. 84, 8487-8519.

TABLE I.

Profile No.	Highest Clouds (km)	Max. Refl. of Clouds	Figure No.	Viking Picno	Filter Color	L_s (deg)	Seasonal Group	Phase (deg)	Latitude at Limb (deg)	Longitude at Limb (deg)
1a	35	0.52	12	005A02	Red	85	B	106	45 N	30
b	35	0.51								
c	38	0.54								
2a	44	0.33	12	005A07	Violet	85	B	106	46 N	31
b	39	0.31								
c	37	0.32								
3a	43	0.34	12	005A10	Violet	85	B	107	32 N	12
b	44	0.37								
c	42	0.38								
4a	30	0.53	13	008A02	Red	87	B	109	49 N	22
b	34	0.56								
c	38	0.56								
5a	48	0.67	13	008A05	Red	87	B	110	35 N	2
b	46	0.66								
c	38	0.65								
6a	33	0.33	13	008A07	Violet	87	B	109	48 N	22
b	41	0.34								
c	38	0.35								
7a	45	0.64	14	022A04	Green	93	B	116	38 N	13
b	46	0.59								
c	46	0.56								
8a	47	0.61	14	022A09	Red	93	B	116	40 N	17
b	49	0.65								
c	47	0.70								
9a	47	0.38	14	022A14	Violet	93	B	116	40 N	17
b	46	0.39								
c	46	0.39								
10a	46	0.47	15	023A05	Violet	96	B	117	37 N	26
b	49	0.47								
c	50	0.46								
11a	50	0.64	15	028A10	Green	96	B	117	37 N	27
b	50	0.63								
c	50	0.62								
12a	56	0.72	15	028A15	Red	96	B	1 7	37 N	28
b	51	0.70								
c	51	0.67								
13a	42	0.17	16	034A11	Violet	99	B	97	47 S	1
b	43	0.18								
c	43	0.18								
14a	42	0.16	16	034A13	Violet	99	B	98	43 S	8
b	45	0.16								
c	46	0.18								

TABLE I (continued).

Profile No.	Highest Clouds (km)	Max. Refl. of Clouds	Figure No.	Viking Picno	Filter Color	L_s (deg)	Seasonal Group	Phase (deg)	Latitude at Limb (deg)	Longitude at Limb (deg)
15a	44	0.26	16	034A29	Red	99	B	96	47 S	2
b	45	0.25								
c	42	0.21								
16a	42	0.31	16	034A31	Red	99	B	97	43 S	8
b	42	0.29								
c	39	0.25								
17a	42	0.29	16	040A03	Violet	101	B	105	43 S	359
b	41	0.28								
c	41	0.28								
18a	40	0.30	17	040A06	Violet	101	B	107	30 S	13
b	40	0.29								
c	40	0.28								
19a	40	0.32	17	040A61	Red	101	B	104	45 S	353
b	41	0.30								
c	40	0.29								
20a	38	0.33	17	040A63	Red	101	B	104	40 S	4
b	38	0.31								
c	38	0.29								
21a	38	0.39	17	040A65	Red	101	B	106	36 S	9
b	41	0.33								
c	41	0.34								
22a	41	0.46	17	040A66	Red	101	B	107	28 S	16
b	41	0.45								
c	41	0.44								
23a	46	0.53	18	060A13	Violet	110	B	126	18 S	352
b	46	0.53								
c	44	0.53								
24a	43	0.39	18	079A11	Violet	120	B	117	49 S	326
b	42	0.39								
c	43	0.38								
25a	38	0.32	18	079A16	Violet	120	B	119	32 S	350
b	35	0.30								
c	38	0.32								
26a	40	0.55	19	085A25	Violet	122	B	124	6 S	251
b	39	0.54								
c	40	0.54								
27a	43	0.40	19	085A44	Violet	122	B	122	37 S	225
b	43	0.39								
c	43	0.36								
28a	21	0.32	19	088A11	Violet	124	B	104	53 S	95
b	22	0.28								
c	23	0.26								
29a	49	0.85	20	101A65	Red	129	B	121	12 S	185
b	49	0.83								
c	48	0.83								

TABLE I (continued).

Profile No.	Highest Clouds (km)	Max. Refl. of Clouds	Figure No.	Viking Picno	Filter Color	L_s (deg)	Seasonal Group	Phase (deg)	Latitude at Limb (deg)	Longitude at Limb (deg)
30a	49	0.52	20	101A68	Violet	129	B	121	11 S	186
b	50	0.50								
c	50	0.52								
31a	46	0.35	20	500A34	Red	357	D	27	1 S	178
b	45	0.35								
c	45	0.36								
32a	24	0.14	21	590A95	Violet	40	A	20	60 S	309
b	22	0.09								
c	22	0.07								
33a	19	0.12	21	590A98	Red	40	A	20	59 S	309
b	20	0.08								
c	20	0.06								
34a	46	0.21	21	605A47	Violet	46	A	28	34 S	163
b	48	0.21								
c	45	0.21								
35a	33	0.28	21	605A48	Red	46	A	28	30 S	162
b	31	0.23								
c	31	0.23								
36a	18	0.14	21	605A94	Red	46	A	25	62 S	174
b	18	0.09								
c	12	0.04								
37a	37	0.27	22	802A09	Red	135	B	74	42 S	226
b	45	0.19								
c	25	0.16								
d	57	0.25								
e	52	0.26								
38a	64	0.25	23	146B02	Violet	185	C	77	39 S	57
b	66	0.23								
c	72	0.23								
39a	67	0.21	23	146B11	Violet	185	C	79	6 N	1
b	68	0.23								
c	67	0.22								
40a	62	0.26	23	146B12	Violet	185	C	79	4 S	15
b	60	0.25								
c	63	0.24								
41a	66	0.21	23	146B39	Violet	185	C	78	23 N	325
b	67	0.21								
c	65	0.21								
42a	63	0.44	22	157B22	Red	192	C	76	32 S	28
b	70	0.45								
c	68	0.45								
43a	70	0.21	23	159B35	Violet	194	C	75	22 N	307
b	69	0.21								
c	67	0.21								

TABLE I (continued).

Profile No.	Highest Clouds (km)	Max. Refl. of Clouds	Figure No.	Viking Picno	Filter Color	L_s (deg)	Seasonal Group	Phase (deg)	Latitude at Limb (deg)	Longitude at Limb (deg)
44a	61	0.36	22	161B22	Red	195	C	74	32 S	140
b	63	0.35								
c	64	0.35								
45a	63	0.42	22	165B22	Red	198	C	71	22 S	230
b	65	0.45								
c	63	0.43								
46a	64	0.54	24	356B19	Red	314	D	74	51 S	133
b	59	0.51								
c	59	0.51								
47a	39	0.24	24	359B19	Red	315	D	76	50 S	56
b	38	0.23								
c	40	0.26								
48a	41	0.51	24	375B35	Red	324	D	81	28 S	61
b	42	0.54								
c	43	0.53								
49a	66	0.54	25	385B39	Red	329	D	86	35 S	127
b	64	0.54								
c	59	0.54								
50a	46	0.56	25	402B11	Red	338	D	97	8 S	56
b	45	0.54								
c	45	0.55								
51a	58	0.52	25	402B23	Red	338	D	97	25 S	37
b	59	0.54								
c	61	0.55								
52a	67	0.56	26	407B13	Red	340	D	97	5 S	4
b	68	0.57								
c	74	0.56								
53a	66	0.55	26	407B27	Red	340	D	98	20 S	344
b	72	0.57								
c	65	0.61								
54a	62	0.60	26	415B11	Red	345	D	103	10 S	309
b	60	0.60								
c	57	0.61								
55a	62	0.61	27	415B31	Red	345	D	102	42 S	259
b	63	0.63								
c	64	0.58								
56a	50	0.65	27	439B14	Red	357	D	115	49 S	85
b	48	0.66								
c	46	0.67								
57a	62	0.79	27	439B22	Red	357	D	117	1 S	159
b	61	0.80								
c	64	0.79								

APPENDIX

Images 1 and 2 (Figure 12). The 4-km-greater height given for violet image no. 2 over no. 1 (red) in Table I is due to a tenuous upper layer invisible in red and barely detectable on the violet image.

Images 4-6 (Figure 13). It is less than 20 km from 6a to 6c, since the frame included only a short section of the limb. Traverse 4a falls between 6a and b.

Images 4 and 6 are the farthest north of the selected images. Both the peaks and troughs of the upper cloud layer lie higher in the violet profiles than in their red counterparts. If real, this would mean that the clouds are not homogeneous in color. We have seen cloud color gradients in more vertical views from both Viking and Earthbased photography, so this phenomenon should not be unexpected in limb views (Martin 1976, 1981a).

The gradation of cloud heights seen on profiles 4a through 4c continues with 5c through 5a. Note that, of the first six frames, nos. 3 (violet) and 5 (red) have the higher clouds. They differ in time by three days, but both show areas to the south and east of the other

four images. This was one of several instances suggesting more correlation with location than with time.

Images 7-9 (Figure 14). The order of the profiles is arbitrary: 7a is in the same direction from the center of the limb as 8c and 9c. The difference between the reflectances of images 8 (red) and 9 (violet) is greater than between other red/violet pairs, except nos. 29 and 30 (Figure 4).

Images 13-16 (Figure 16). These four images have less reflectance than the earlier twelve images, which had slightly higher phase angles as well as being in the northern hemisphere. Figures 5 and 6 suggest that phase is the more dominant variable.

Images 21 (Figure 17). The limb position for no. 21 is probably incorrect by about 2 km due to the limb being very near to the center of the image; that situation affects the accuracy of the computer program that determines the limb. Several other images whose centers were off the limb were rejected from the study. We believe the peaks of these profiles should coincide approximately with the limb.

Image 22 (Figure 17). The bright layer 15 km above the limt on image 22 is one of the two cases where red-filter images were found to have upper layers of clouds with greater reflectances than those recorded at the limb. The other case is profile 55b. This also occurs on several violet images.

Image 23 (Figure 18). Like several other violet images, these profiles increase in reflectance going from the planet's center toward the limb and then level off at the limb. On 23c the peak reflectance is greater than seen at the limb. Among the selected violet-filter images, 23a and 23b are the only profiles with reflectances above 0.5 at the limb.

Images 24-25 (Figure 18); Images 26-27 (Figure 19). The shapes of the profiles indicate major differences in the structure of the limb clouds. Image 24 has a very bright upper layer with a large gap between it and the clouds at the limb, while 25 has a more uniform band of clouds above the limb in which layering is only minor.

Both 25 and 26 are of areas more to the north than 24 and 27, and both show less layering than their more southerly counterparts. The two pairs are separated from each other by more than 100° of longitude and six days in time. The multiple layers on traverse 27c produced the most sawtoothed profile of the entire study. Both nos. 26 and 27 have

greater reflectances above the limb than at the limb.

The camera signal offset was not inhibited on images 24-27, possibly affecting the profiles as discussed earlier in this paper.

Image 28 (Figure 19). The height of these limb cloud tops is the lowest among the selected violet images. However, the existence of higher cloud layers cannot be ruled out; if faint, they may have failed to be detected because the camera signal offset was not inhibited for this exposure. Error in the calculated location of the surface limb (based on 12 craters in this frame) could also play a role, but probably a minor one.

Images 29 and 30 (Figure 20). Of the selected red/violet pairs, these have the greatest differences in reflectance. Image 29 has the largest reflectance of those measured and also has the highest phase angle of the selected red-filter images (Figure 6). These images cover latitudes that are known to encompass dust storm activity (Martin, 1974, 1976).

Image 31 (Figure 20). This Viking Orbiter 1 image was taken 50 minutes

earlier on the same day that Viking Orbiter 2 took image 57. They show neighboring areas of Mars but were taken in nearly opposite directions (Figure 2). We suggest that difference in phase angle is the primary reason for the large differences in reflectance between nos. 31 and 57 (Figure 7). This possibly can also account for the 17 km difference in height as well. No. 31 has the greatest cloud height of any image selected with a low phase angle. The limb positions for no. 31 could be inexact because only nine control point craters were usable, but that error probably is no more than 5 km.

Images 32 and 33 (Figure 21). The individual profiles 32a-c and 33a-c illustrate the effects of very small changes in either phase angle and/or latitude. The "a" profiles have the higher phase angles and are further north, whereas the "c" profiles have the lower phase angles and are further south. On both images there is a definite progressive decrease in reflectance but only minimal changes in height as the traverses both moved toward the south and their phase angles decreased.

Images 34 and 35 (Figure 21). This is the only red/violet pair in which the violet profiles peak in reflectance at the limb while the

red profiles slope down in reflectance as they cross the limb. The profiles portray the greatest height differences between all selected color pairs (12 to 27 km).

Image 36 (Figure 21). This is the most southerly image in this study. The phase angles are less than for the above pair, and the individual profiles have progressively smaller phase angles as they increase in southerly latitude, from "a" to "c." Profile 36c is one case where both the cloud height and reflectivity decrease with a minor decrease in phase; however, the latitude could be a controlling variable.

Image 37 (Figures 1 and 22). The limb clouds shown on the Figure 1 photograph are possibly the most spectacular in appearance that were recorded during the entire Viking mission and show more variation than any of the other selected pictures. They are relatively low in reflectivity and vary in height from 25 to 57 km above the limb. This is chronologically the last frame in this study and the only one that extends beyond the first Martian year of the mission (southern Martian winter). It is the only selected picture that faces almost directly south (Figure 2).

Profile 37d traverses the brightest part of the clouds, with "b"

and "e" close by on either side. No. 37a is east of the main cloud (left on Figure 1), while "c" is to the west of it.

Image 43 (Figure 23). From 20 km below the limb to 20 km above the limb, these are the flattest profiles of this study.

Image 44 (Figure 22). Only nine control craters were used for determining the limb position.

Image 46 (Figure 24). This picture is the furthest south in Seasonal Group D and is the only selected image south of 45° to show cloud heights above 50 km.

Image 47 (Figure 24). This frame has both lowest reflectances and lowest heights of the selected images in this season (D). This can probably be attributed to underexposure of the limb clouds and possibly because the camera signal was offset, as mentioned earlier in this paper. These profiles should be compared to those on Figure 21, which were also weak but due to low phase angles, rather than

underexposure. The shape of the no. 47 profiles gives a bolder definition to the limb clouds, whereas the Figure 21 profiles portray clouds that fade as they rise above the limb. The only profiles that look even slightly similar to no. 47 are those of no. 28, which also may have been affected by camera signal offset.

Image 49 (Figure 25). The brighter clouds go up to only about 35 km above the limb, but with another prominent layer above it that peaks near 40 km. Higher but fainter upper layers appear irregular, disconnected, and difficult to resolve within the noise.

Images 50 and 51 (Figure 25). In this case we believe that the location on Mars is the primary variable between these same-day images, even though they are not far apart. No. 50 looks across Vallis Marineris toward the northwest, whereas no. 51 shows an area to the southeast. The canyon appeared to have been filled with bright clouds, possibly similar to the morning hazes discussed by Briggs et al. (1977). These two images differ in cloud height by 14 km but have nearly the same reflectances.

Images 52 and 53 (Figure 26). This pair of images boasts the highest limb clouds recorded in the study. The highest cloud is on no. 52c at 74 km, with no. 53b just 2 km lower.

Image 55 (Figure 27). Profile 55b is an example of a reflectance peak above the limb that has more reflectance than seen at the limb. See image 22 profiles for the only other clear case of this phenomena. Although the profiles are generally flat at the limb, there is a distinct trough just below the limb on 55c that is believed to be a crater or other topographic feature. On the other hand, the trough above the limb on the same profile represents a break between cloud layers.

Images 56 and 57 (Figure 27). The final pair was taken just 4 minutes, 8 seconds apart. These limb cloud differences are assumed to be due primarily to their widely separated locations on Mars. The upper layer of clouds shown on the no. 56 profiles is the most prominent amongst the selected images in terms of having the deepest drop in reflectance beneath its peaks. Image 57 has a notably higher reflectivity than no. 56 and second only to no. 29, which is both facing in the same direction and covering a nearby location (Figure 2).

FIGURE CAPTIONS

Figure 1. This example photograph illustrates an assortment of limb cloud forms. As a single image, it is not really typical of the limb pictures used in this study, since none of the others has such a complex cloud pattern on the horizon. The circles denote the control craters that were measured to determine the locus of the surface limb. The large crater in the foreground is Herschel. This is image no. 37 of this study. Its limb cloud profiles appear on Figure 22.

Figure 2. The tips of the pointers are the limb locations of all the images used for this study. These pointers also indicate the directions from which the Viking orbiters viewed those limbs. The numbers of overlapping images have been omitted: No. 1 includes no. 2, no. 4 includes no. 6, no. 7 includes nos. 8 and 9, no. 10 includes nos. 11 and 12, no. 13 includes no. 15, no. 14 includes no. 16, no. 17 includes no. 20, no. 29 includes no. 30, no. 32 includes no. 33, and no. 34 includes no. 35. The base map is from the Lowell Observatory Map Series (Inge, 1973).

Figure 3. The latitude distribution of limbs investigated in this study. Earth-calendar months are shown on the abscissa, starting near the beginning of the orbital mission and ending more than two years

later. Martian seasons are shown across the top in terms of L_s. Because of the bunched distribution of the selection, we have grouped the images into seasons lettered "A" through "D." Note that "A" was assigned to the numerical beginning of the Martian year (vernal equinox). Season B includes parts of two Martian years.

Figure 4. Limb cloud reflectances and maximum heights are plotted against Martian season, represented by L_s. As on Figure 3, they are in chronological order, with Earth-calendar months shown across the bottom. The values used are those for the "b" profile for each image. See Table I for the values for all of the profiles. Image 37 has the widest range of values for both height and reflectance. As a general rule, the difference between reflectances in red/violet pairs increases with greater total values in reflectance.

Figure 5. The dependence of reflectance upon phase angle for violet-filter images. All of the violet-filter data are plotted together in this figure, because no evidence is seen for a seasonal variation like that found in the red-filter data plotted in Figures 6 and 7. The five images from Seasonal Group C are clumped together near 78° phase, providing an example of the effects of weak distribution of the selection.

Figure 6. The dependence of reflectance upon phase angle for red-filter images during the half of the Martian year when $0° < L_s < 180°$. This plot more closely resembles the violet-filter plot in Figure 5 than it does the red-filter plot for the other half of the Martian year shown in Figure 7.

Figure 7. The dependence of reflectance upon phase angle for red-filter images during the half of the Martian year when $180° < L_s < 360°$. This sample largely represents the "dust storm season" of a particular Martian year. All but three points in this diagram were for locations in the southern hemisphere. Figures 5-7 suggest plausible phase functions, but one must bear in mind that effects due to latitude, longitude, and season (except for the division into Figures 6 and 7) remain buried in these data and are not random with phase angle.

Figure 8. Heights of cloud tops plotted against phase angles. The "D" season has been outlined only to identify points by season. This outline is not intended to suggest any correlations. The four points marked "high latitude" are all south of -52° latitude; three of these points also are from the images having the lowest phase angles.

Figure 9. Cloud reflectance versus latitude. North and south latitudes

are superimposed in this figure and in Figure 10. The northern hemisphere was poorly represented in our sample (see Figures 2 and 3), but no systematic difference between hemispheres was apparent.

Figure 10. Heights of cloud tops versus latitude. See the caption for Figure 9 for additional applicable comments.

Figure 11. Comparing the reflectance with cloud-top heights, we see that higher is not always brighter. The "C" season data are identified, because the points for that season are clustered in one corner of this diagram.

Figure 12. Revolution 5A. Images 1 and 2 overlap. (One of 11 overlapping red/violet pairs.) Image 3 adjoins them.

Figure 13. Revolution 8A. Images 4 and 6 overlap; image 5 adjoins them, but the order of profiles is reversed: 5c is next to 4c.

Figure 14. Revolution 22A. One of two sets of three overlapping filter colors (see Figure 15 for the other set).

Figure 15. Revolution 28A. Second of two sets of three overlapping filter colors (see Figure 14 for the other set).

Figure 16. Images 13-16: Revolution 34A; image 13 overlaps 15; 14 overlaps 16. Image 17: Revolution 40A, overlaps image 20 (Figure 17).

Figure 17. Revolution 40A. Image 18 overlaps 22; 20 overlaps 17 (Figure 16); 19a adjoins 20c; 20a adjoins 21c; 21a adjoins 22c.

Figure 18. Image 23: Revolution 60A. Images 24 and 25: Revolution 79A; do not adjoin.

Figure 19. Images 26 and 27: Revolution 85A; do not adjoin. Image 28: Revolution 88.

Figure 20. Images 29 and 30: Revolution 101A, overlapping pair. Images 34-36: Revolution 605A; 34 overlaps 35; 36 does not adjoin them.

Figure 21. Images 32 and 33: Revolution 590A, overlapping pair. Images 34-36: Revolution 605A; 34 overlaps 35; 36 does not adjoin them.

Figure 22. Image 37: Revolution 802A; profiles are ordered east to west from the top. Image 42: Revolution 157B. Image 44: Revolution 161B. Image 45: Revolution 165B.

Figure 23. Images 38-41: Revolution 146B; 39 adjoins 40; others do not

adjoin. Image 43: Revolution 159B.

Figure 24. Image 46: Revolution 356B. Image 47: Revolution 359B (underexposed). Image 48: Revolution 375B.

Figure 25. Image 49: Revolution 385B. Images 50 and 51: Revolution 402B; do not adjoin.

Figure 26. Images 52 and 53: Revolution 407b; do not adjoin. Image 54: Revolution 415B (also image 55, Figure 27).

Figure 27. Image 55: Revolution 415B; does not adjoin image 54 (Figure 26). Images 56 and 57: Revolution 439B.

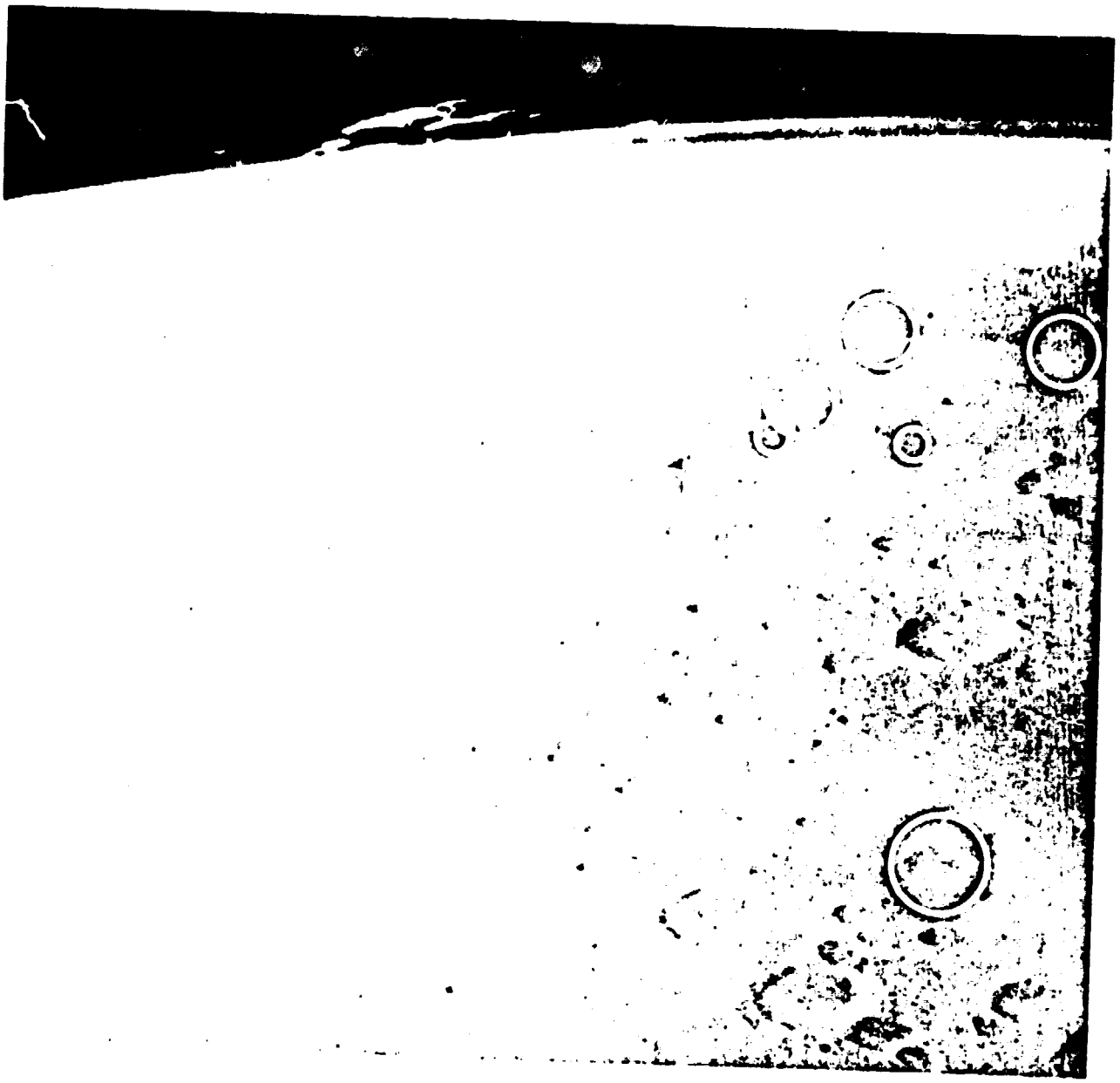

L J MARTIN

Figure 1

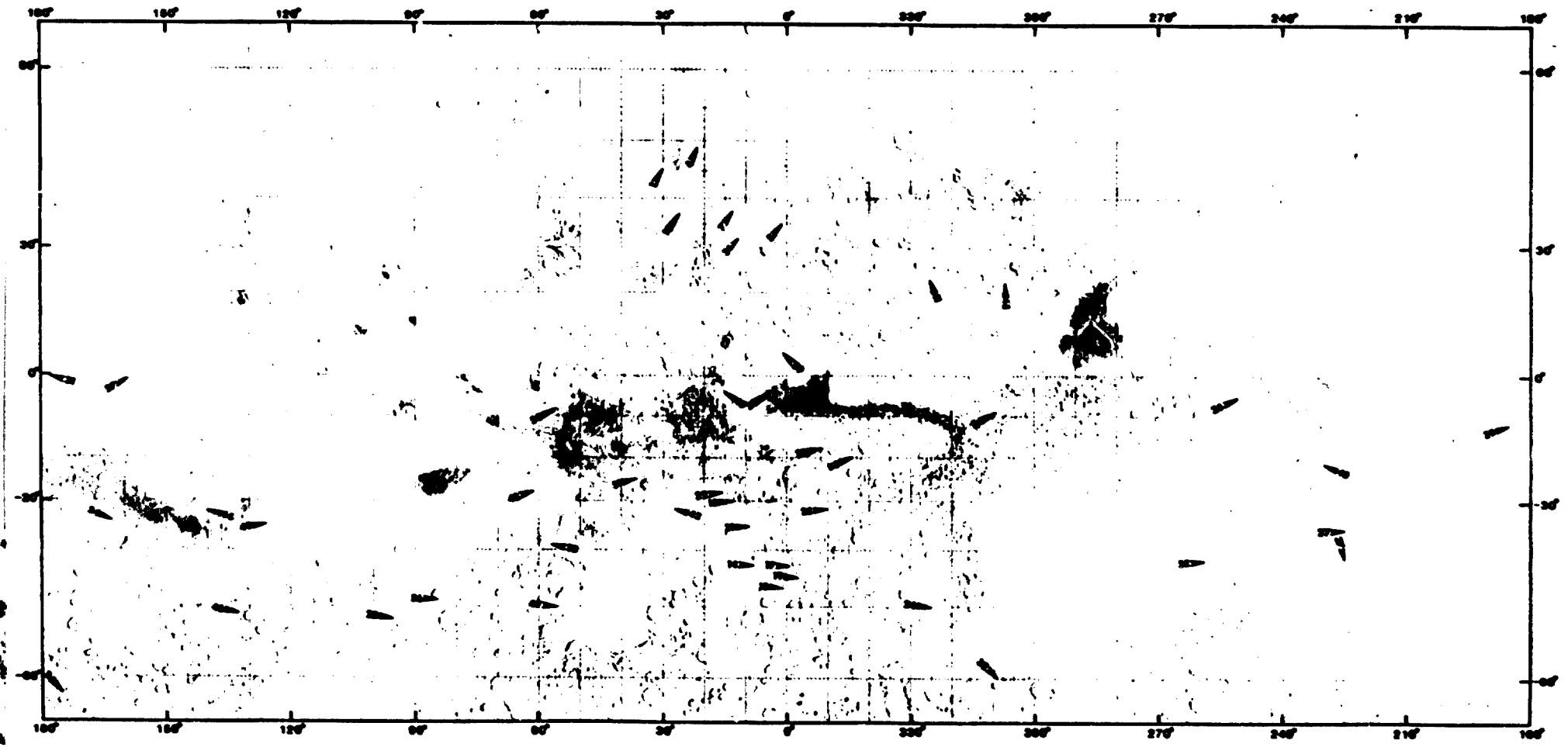

L J MARTIN
Figure 2

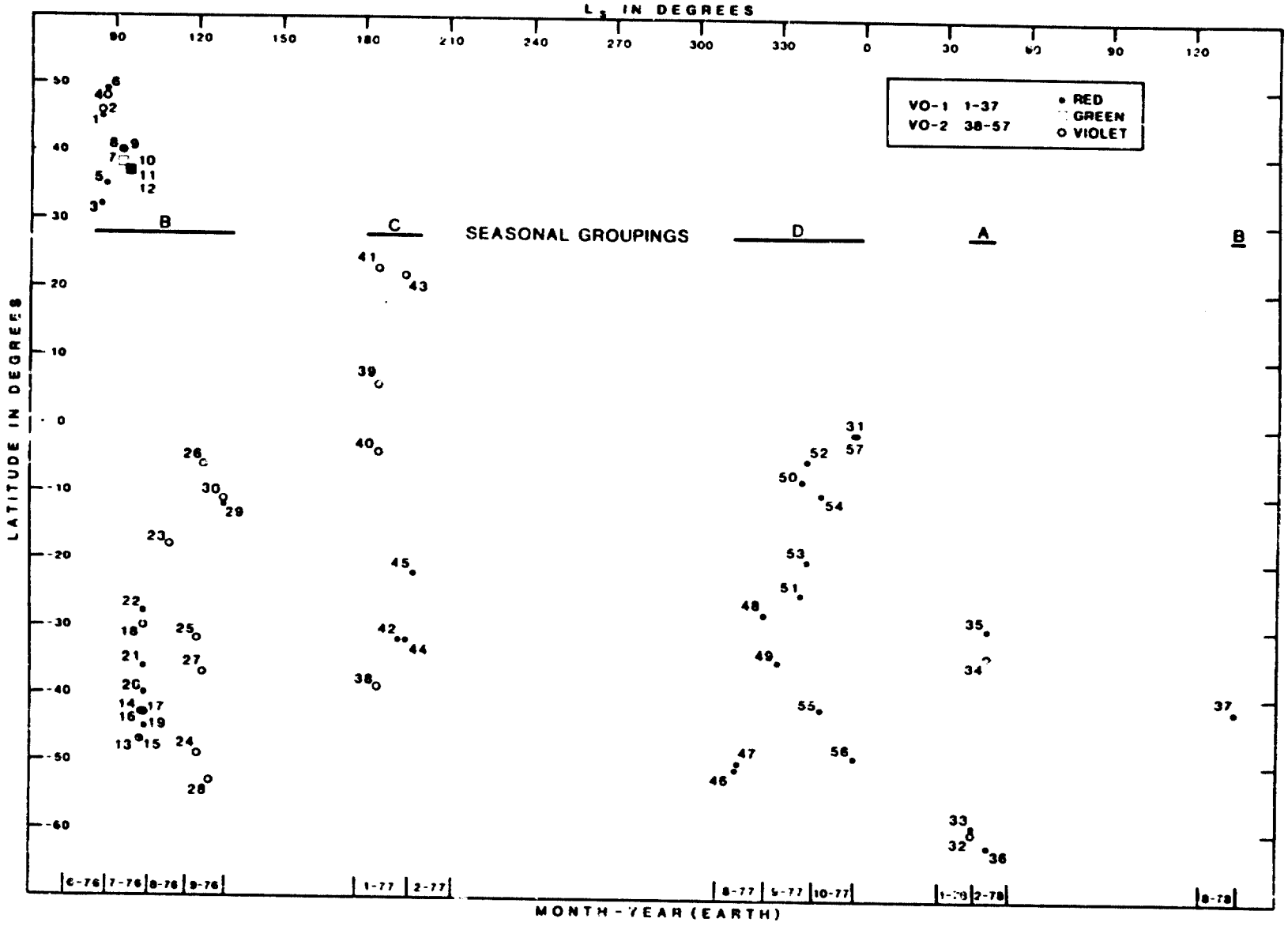

ORIGINAL PAGE IS
OF POOR QUALITY

L J MARTIN
Figure 3

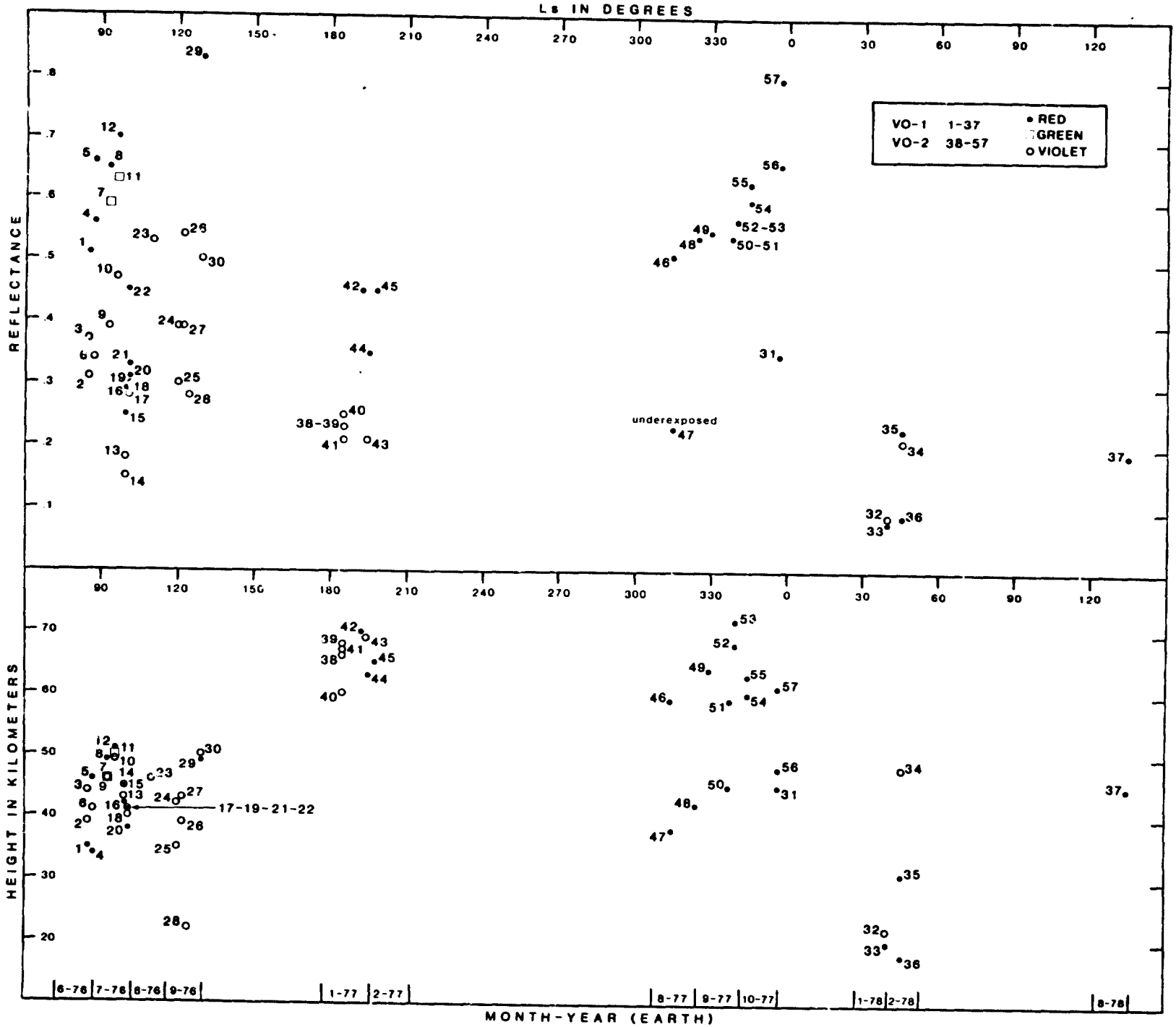

J MARTIN

Figure 4

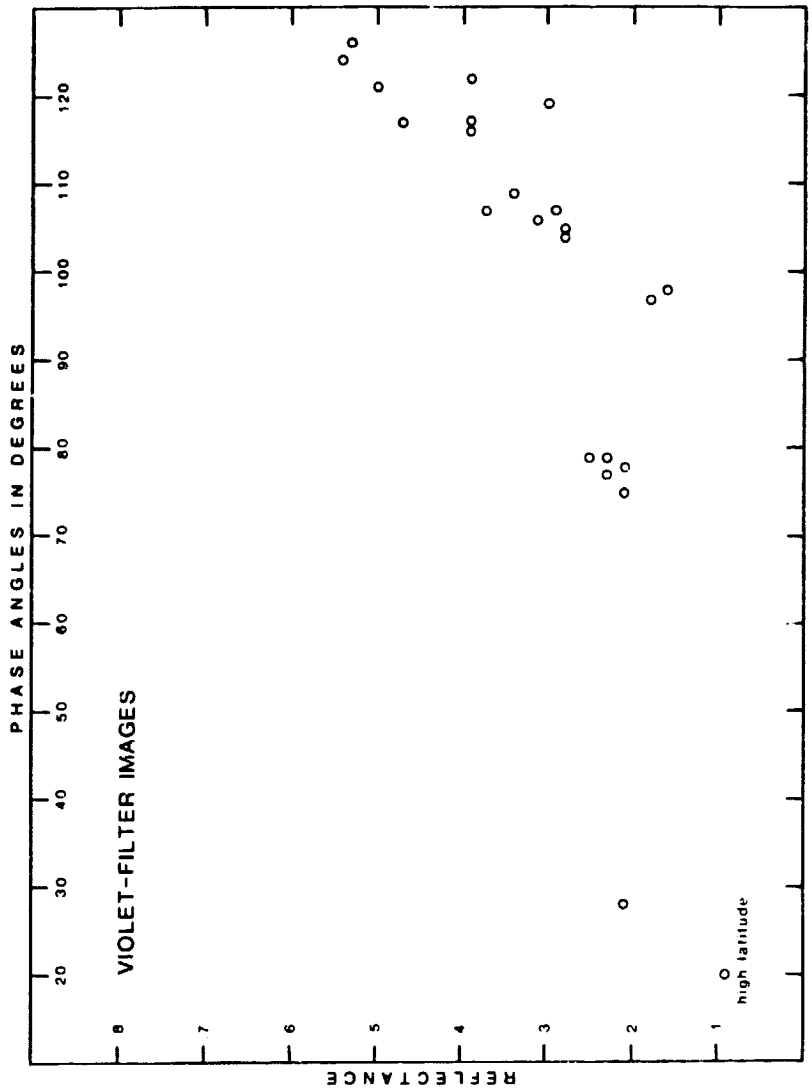

L J MARTIN
Figure 5

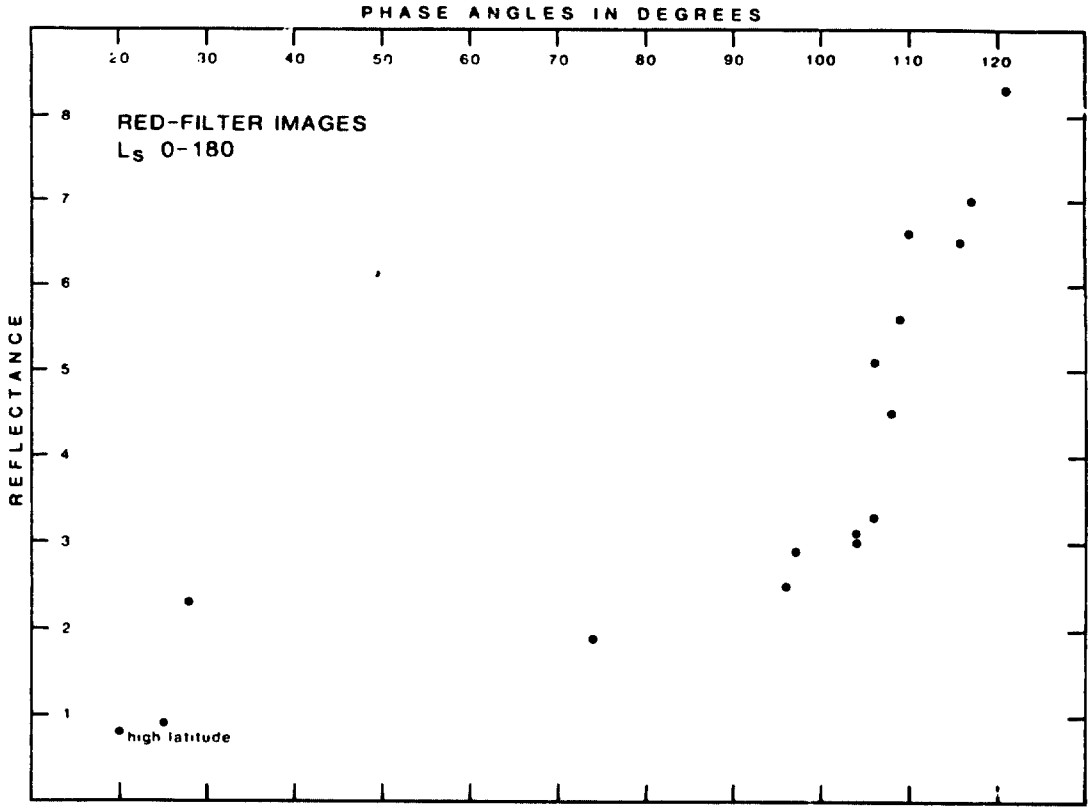

L J MARTIN
Figure 6

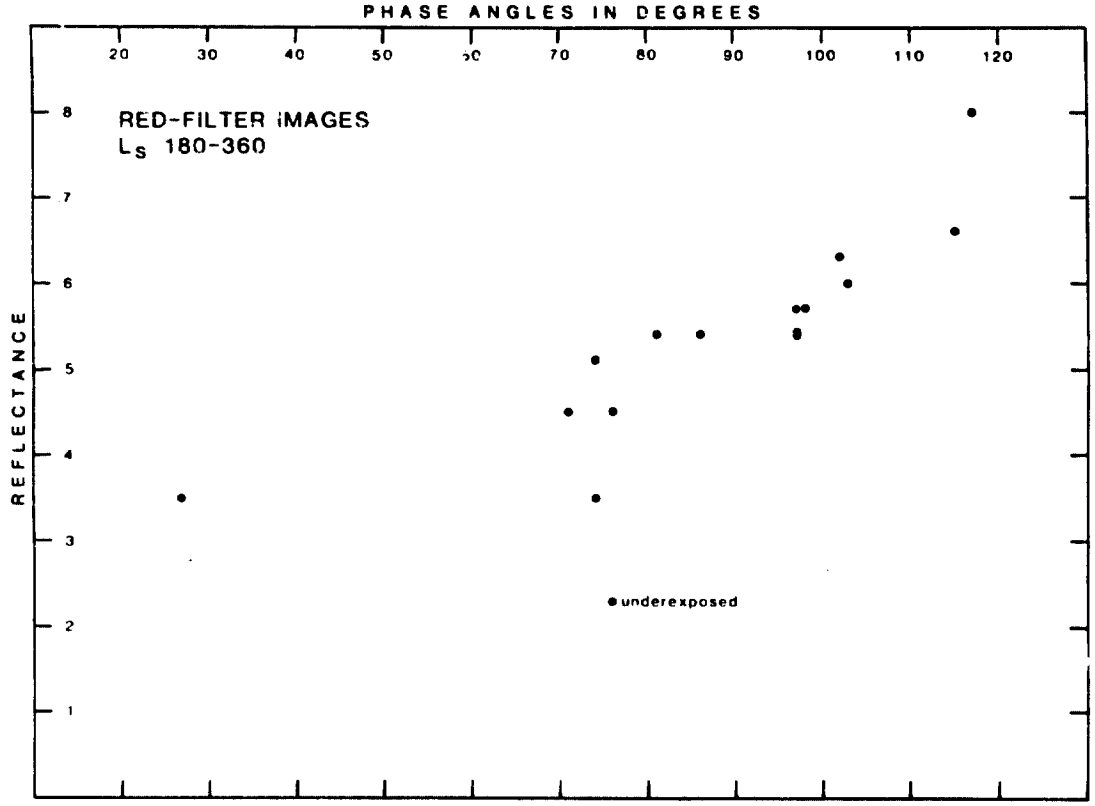

L J MARTIN
Figure 7

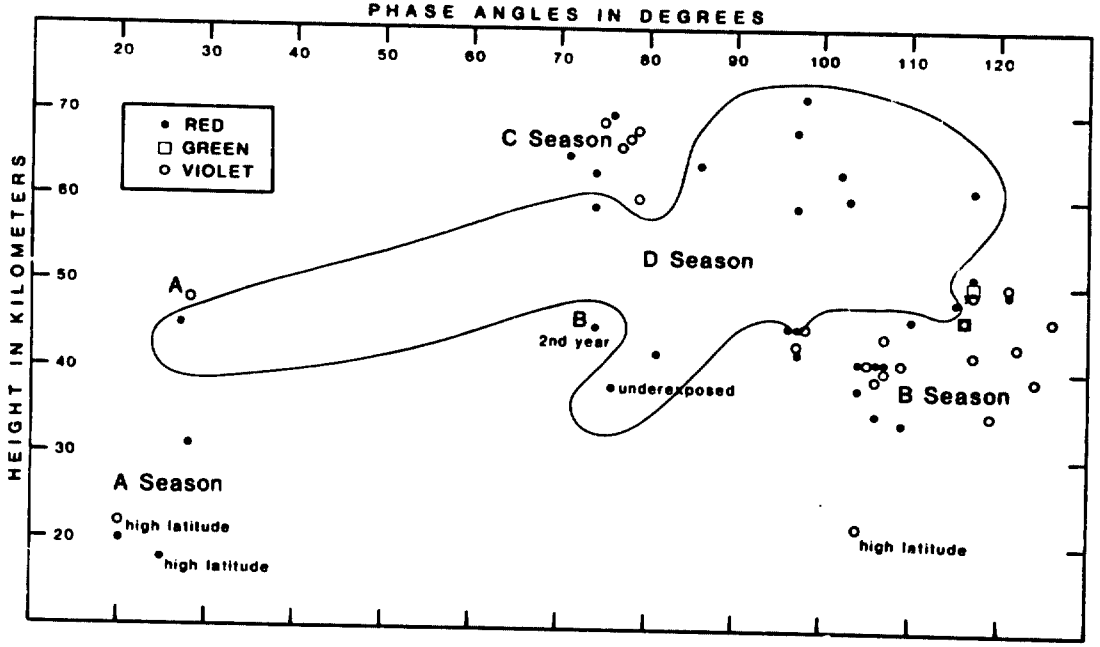

L J MARTIN
Figure 8

L J MART
Figure 9

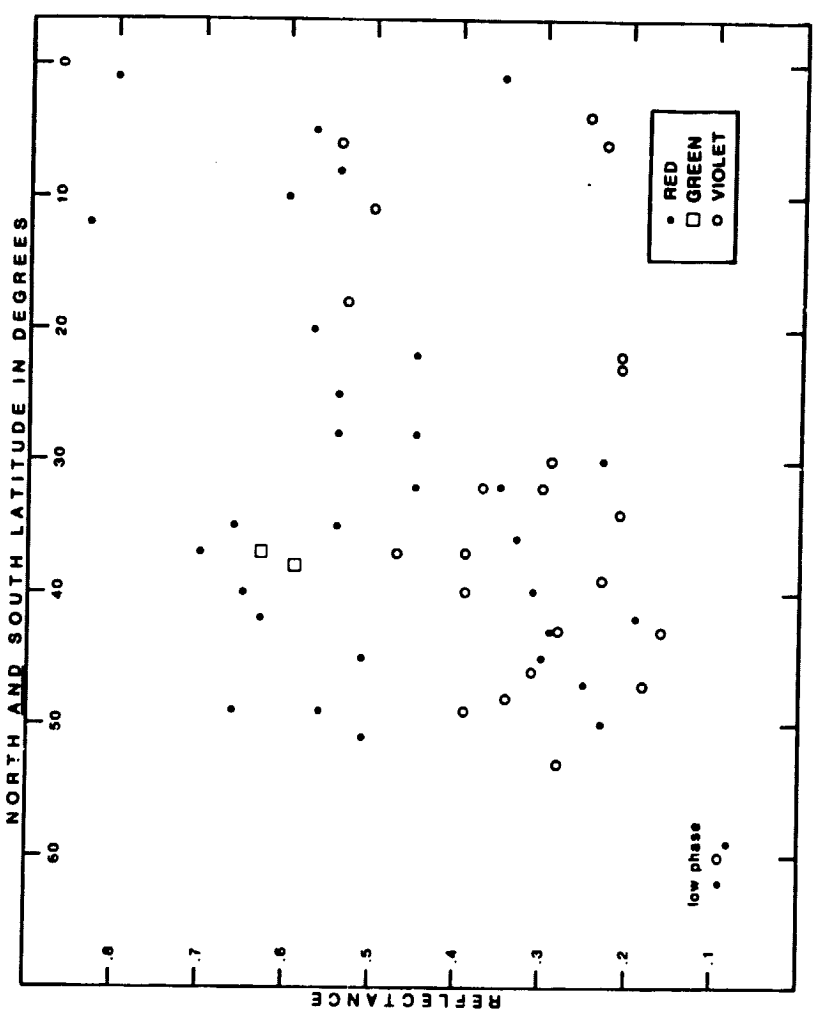

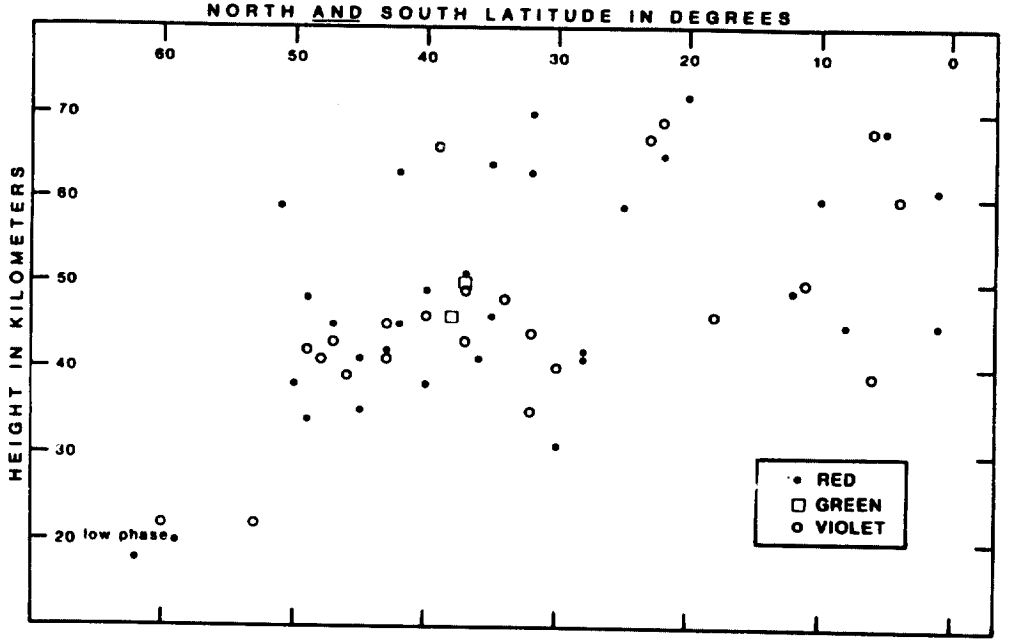

L J MARTIN
Figure 10

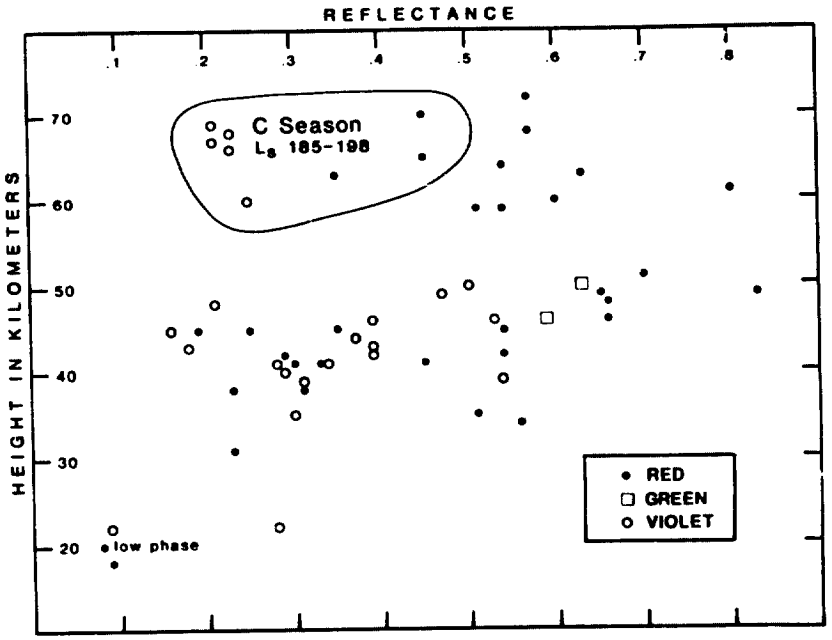

L J MARTIN
Figure 11

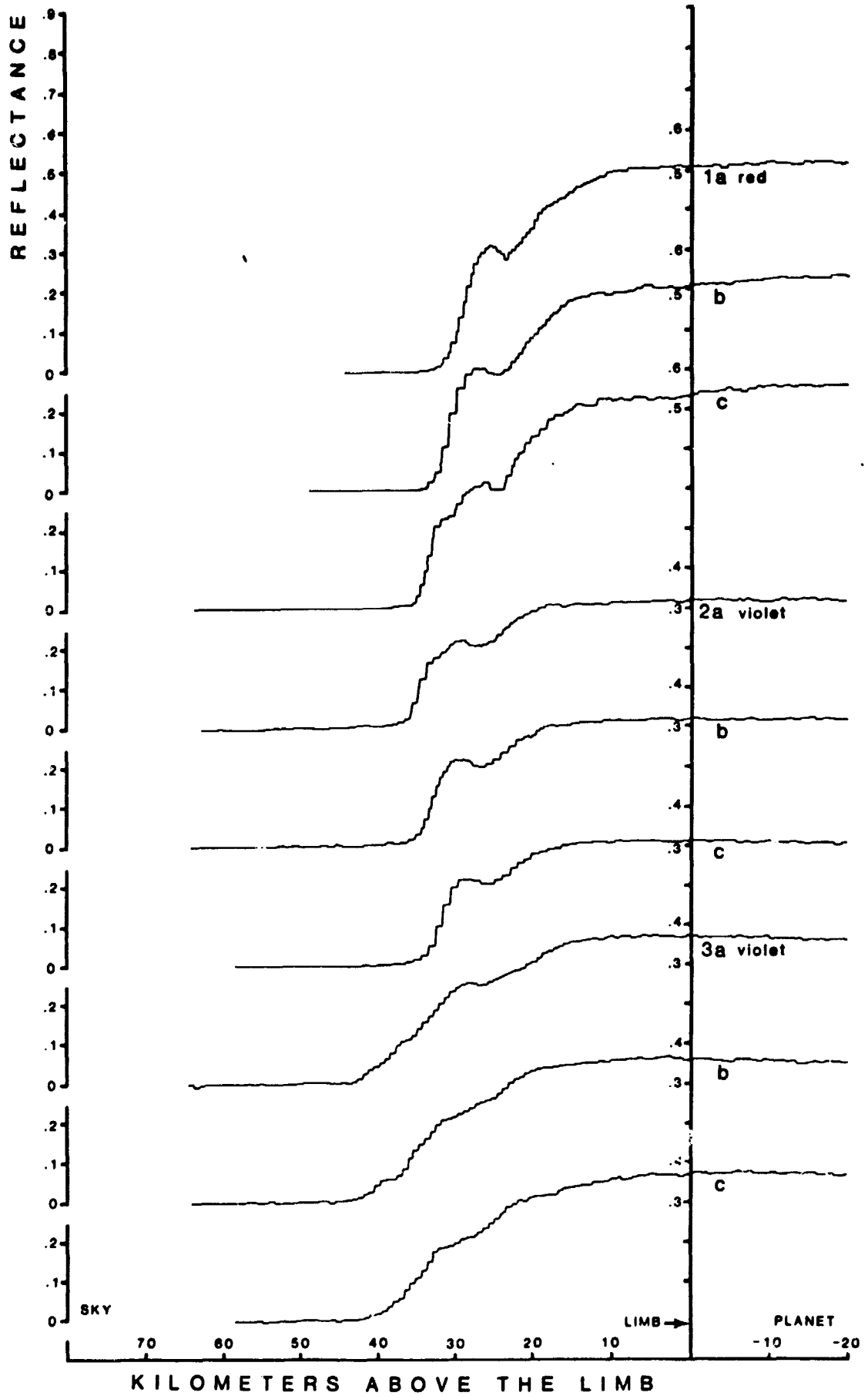

L J MARTIN

Figure 12

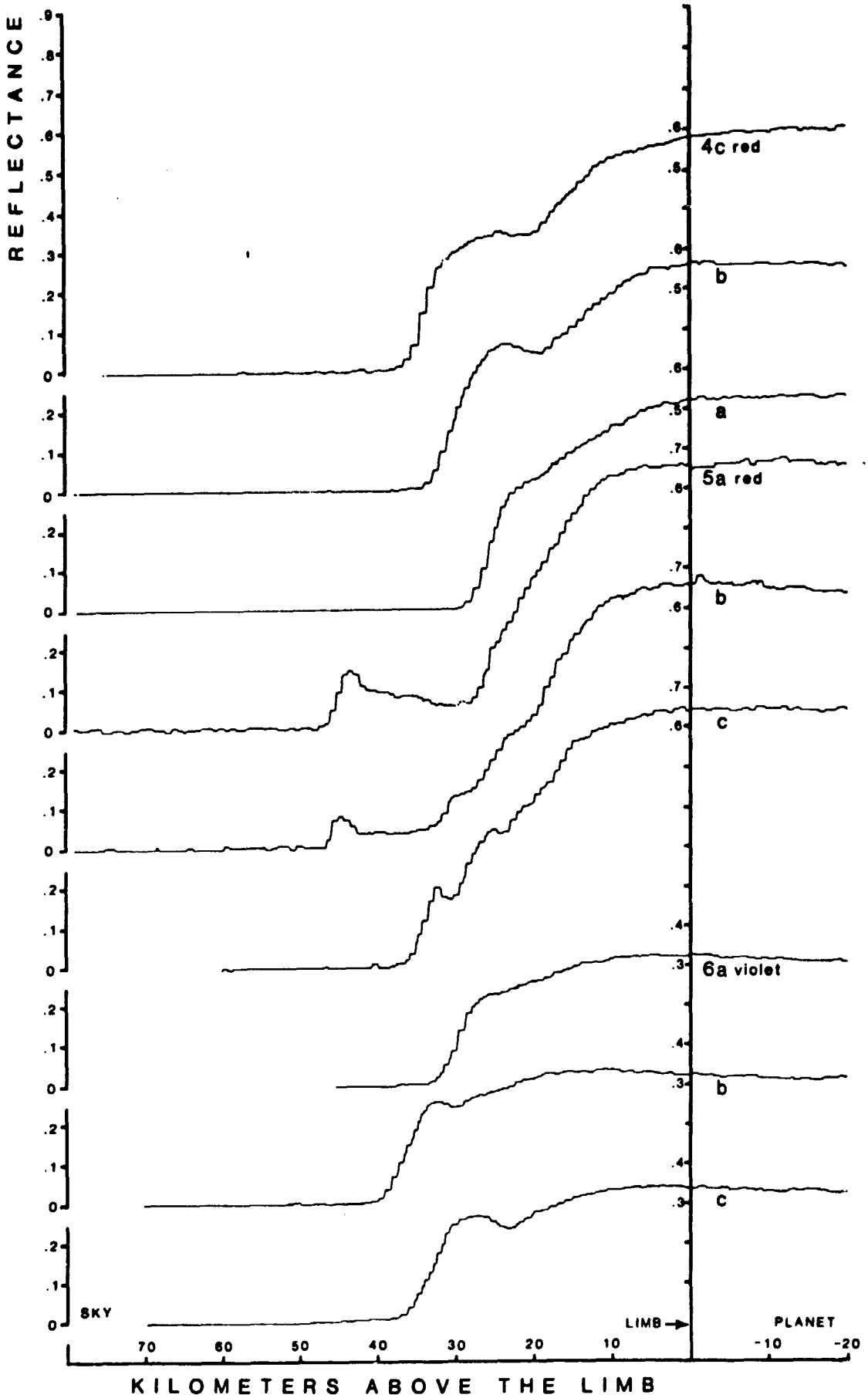

L J MARTIN

Figure 13

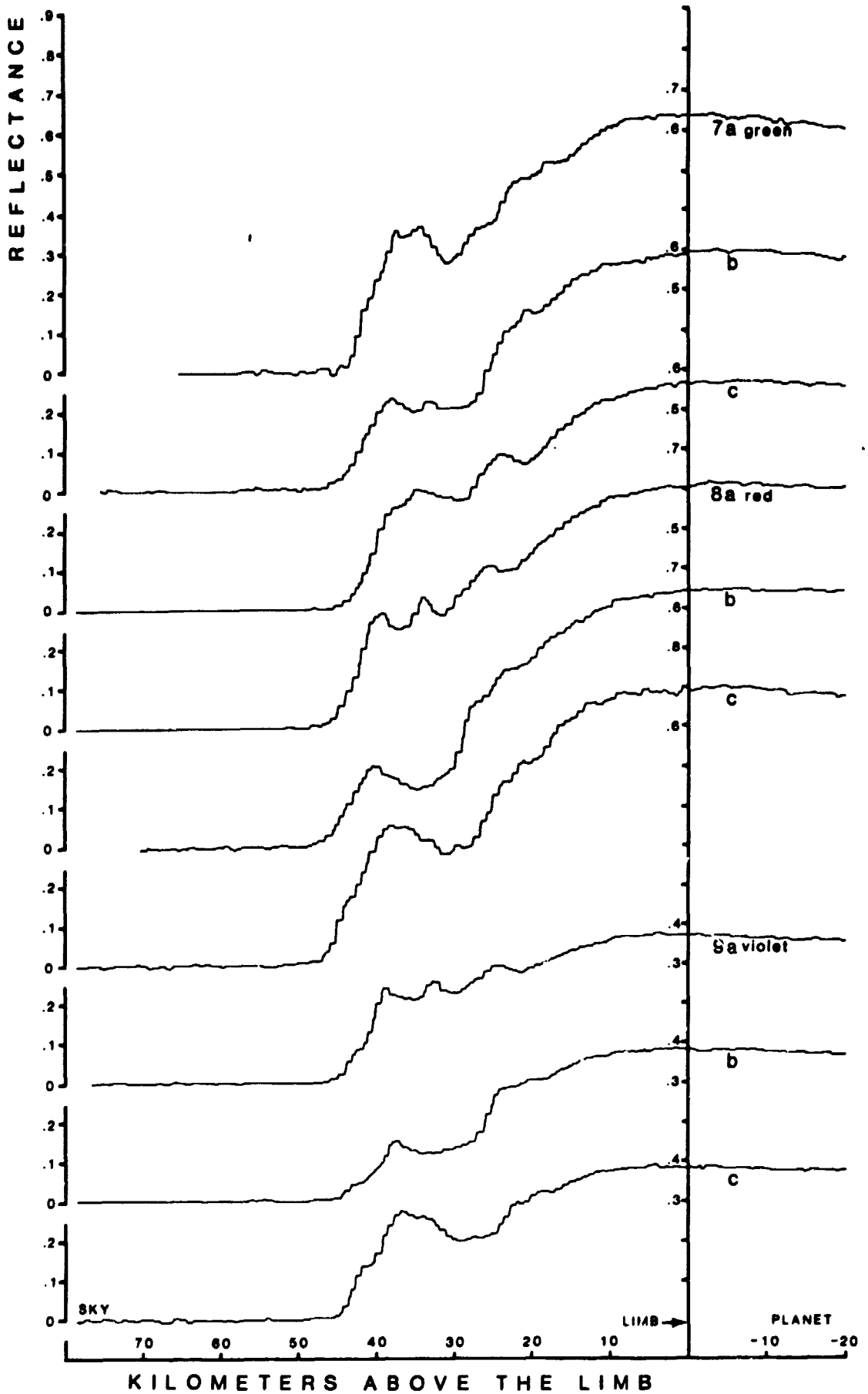

L J MARTIN

Figure 14

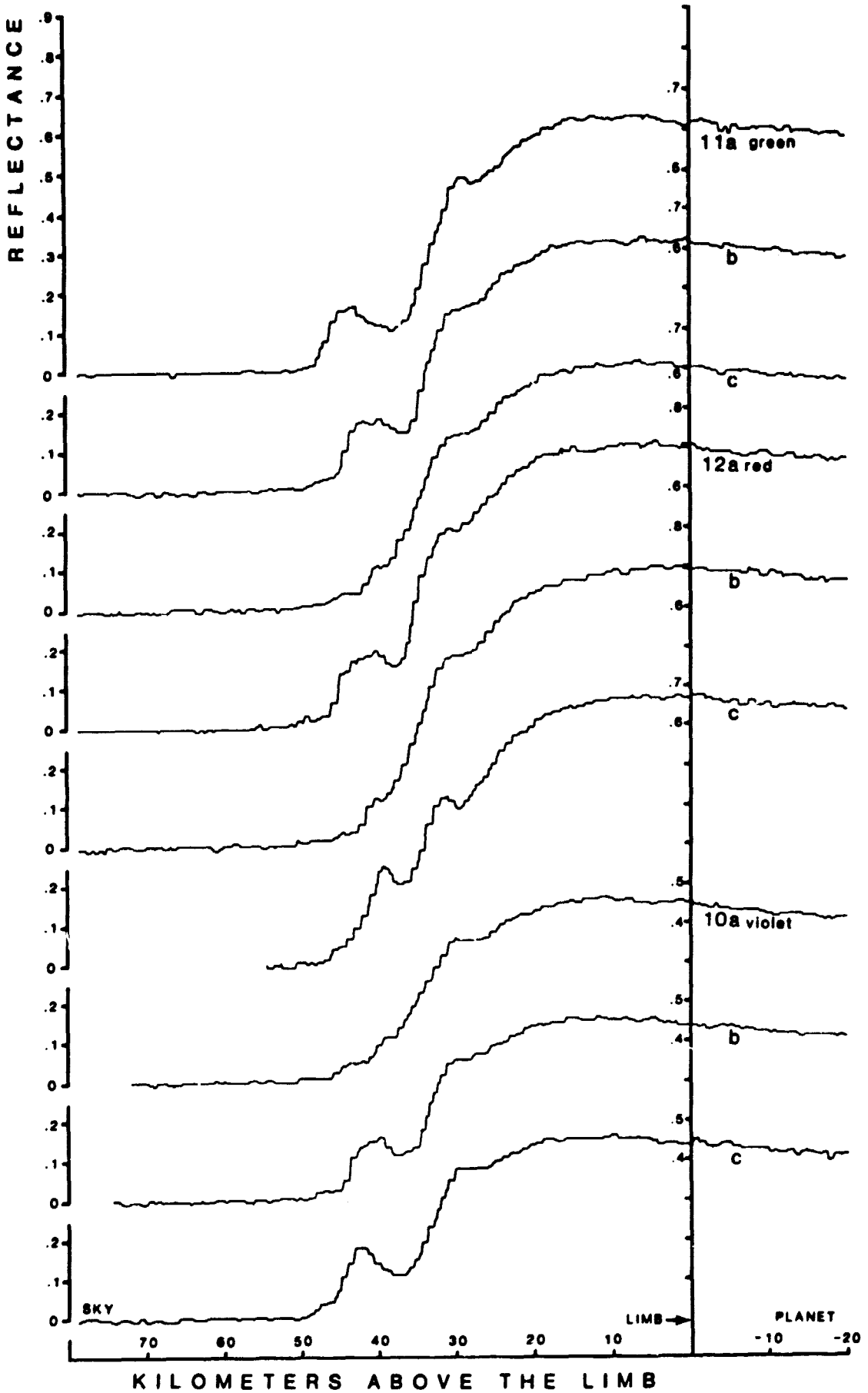

L J MARTIN

Figure 15

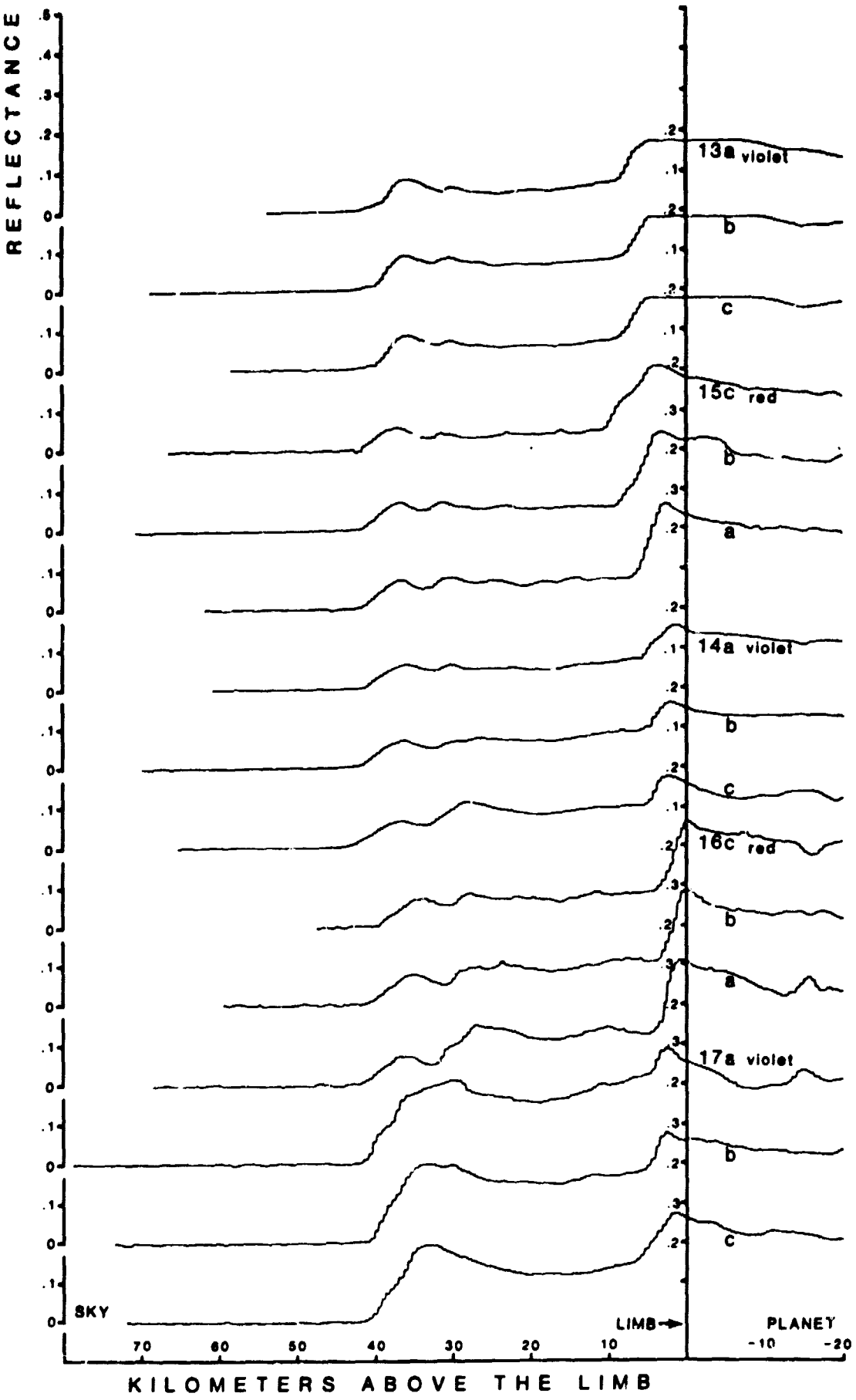

L J MARTIN

Figure 16

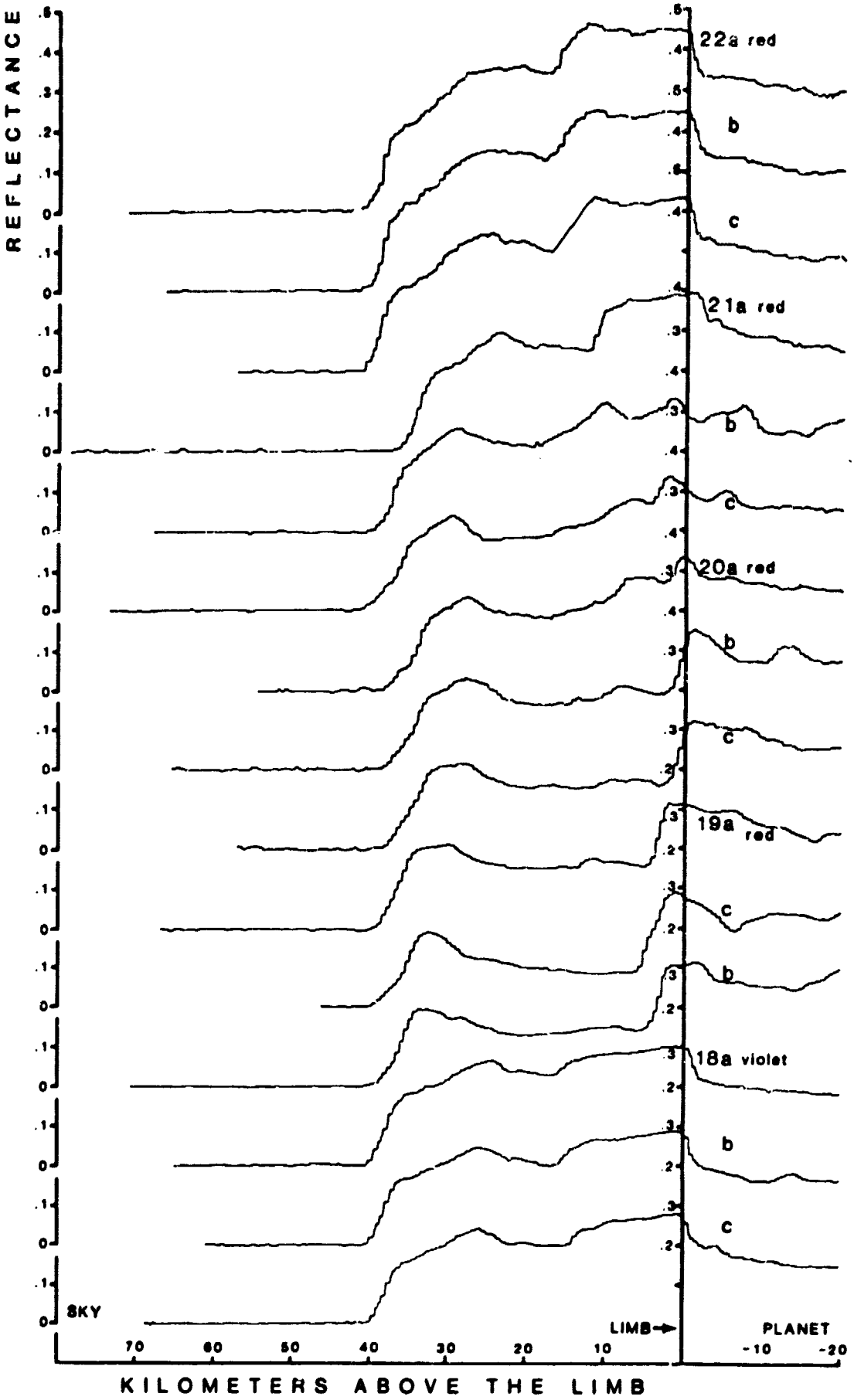

L J MARTIN

Figure 17

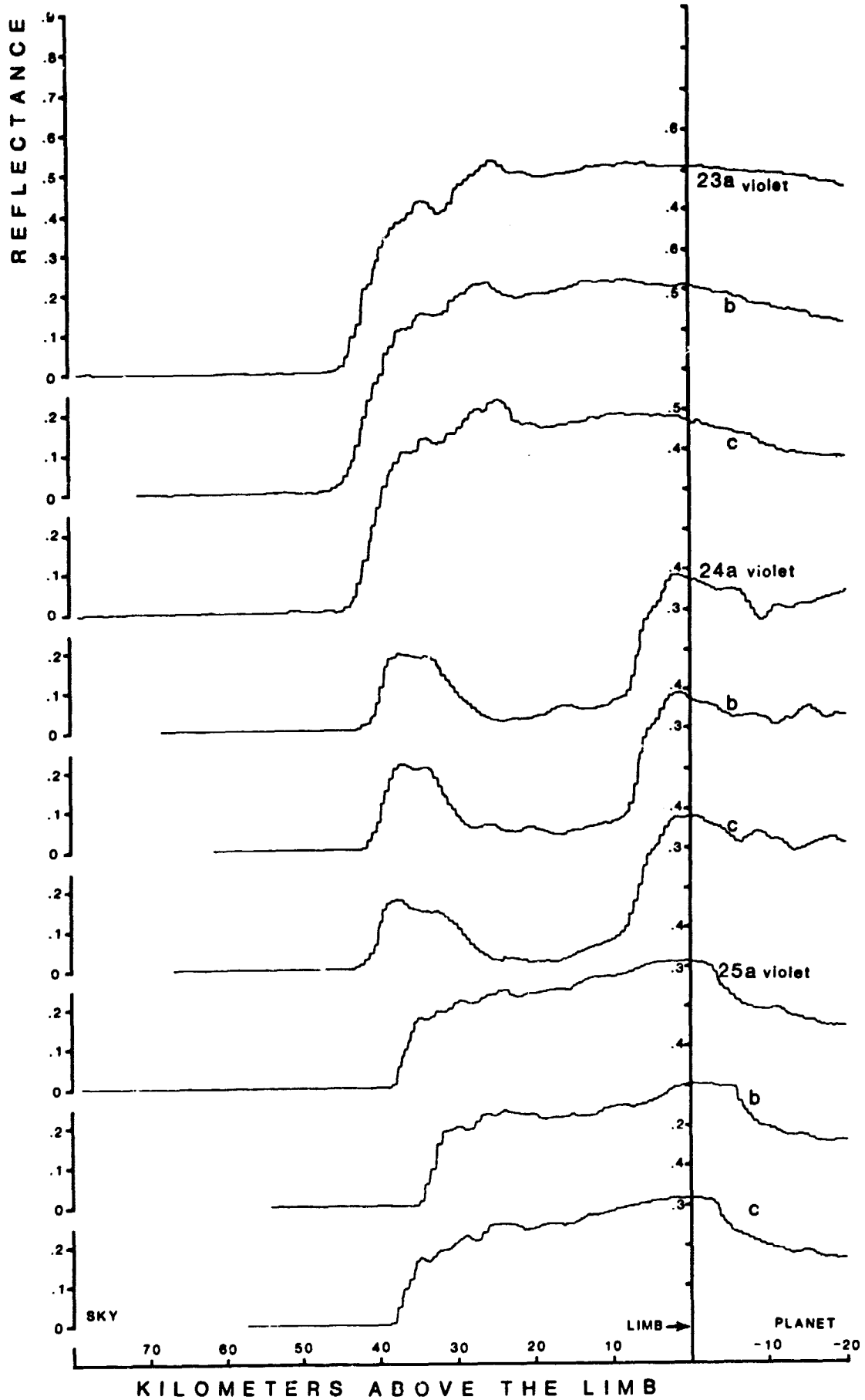

L J MARTIN

Figure 18

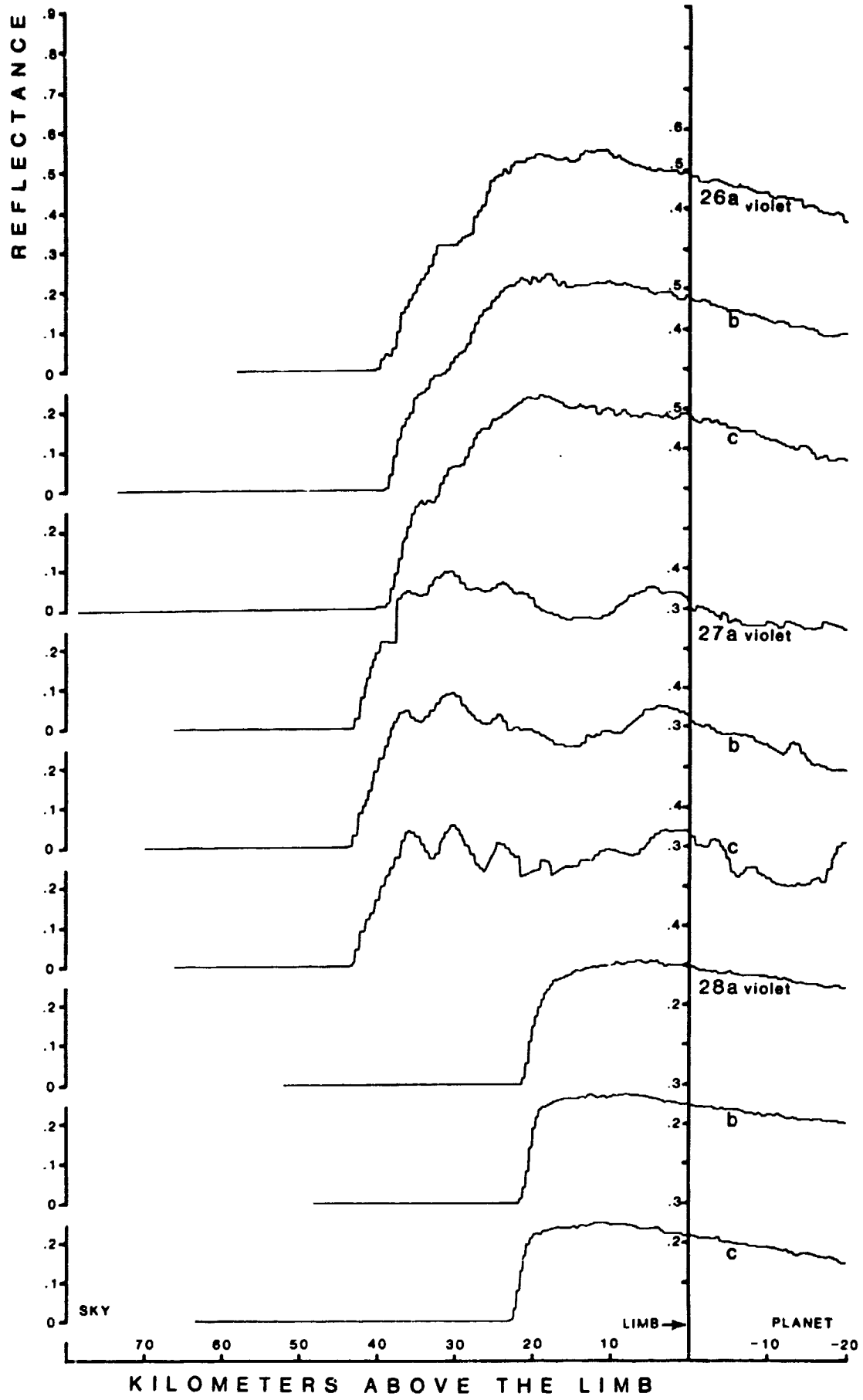

L J MARTIN

Figure 19

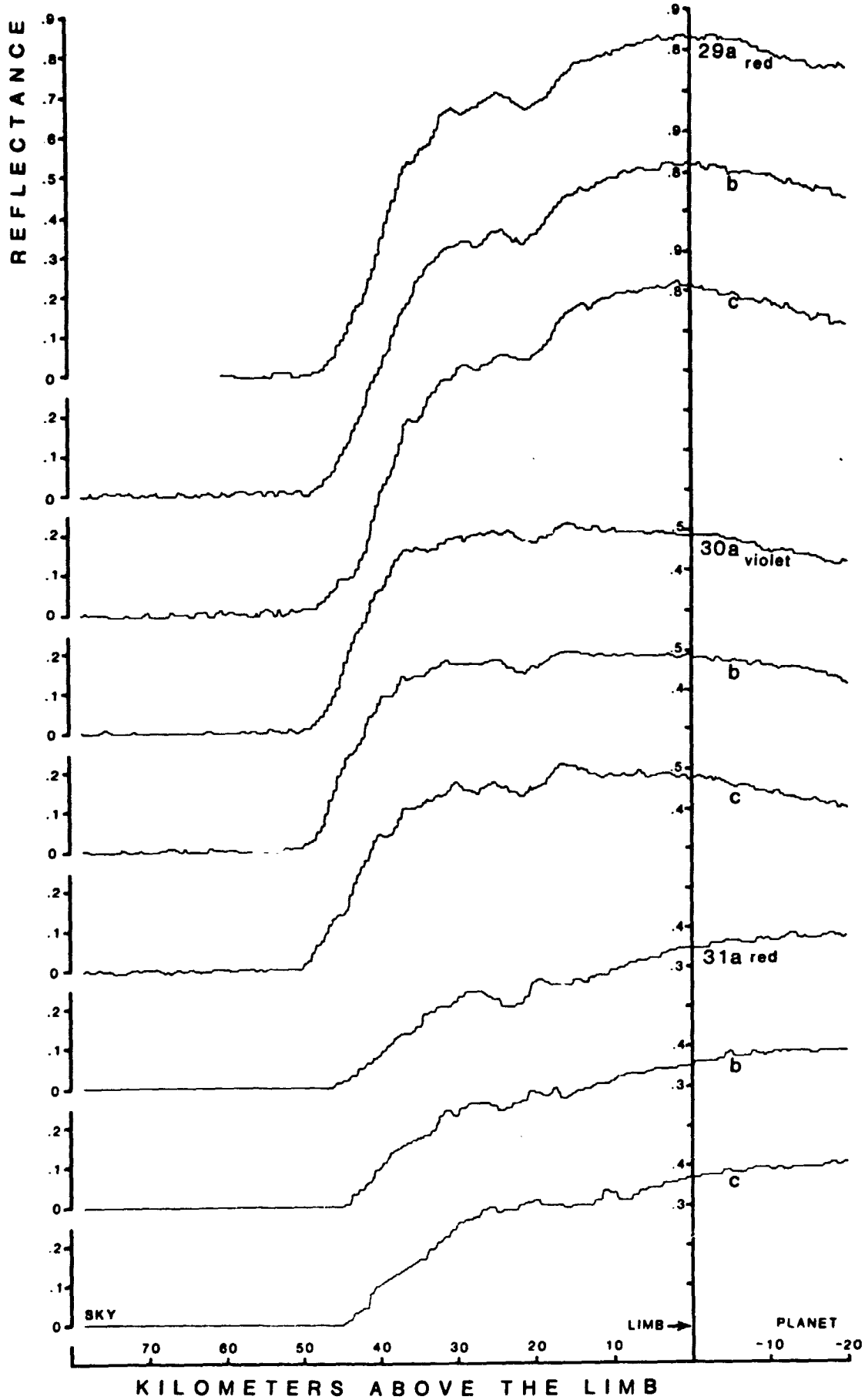

L J MARTIN

Figure 20

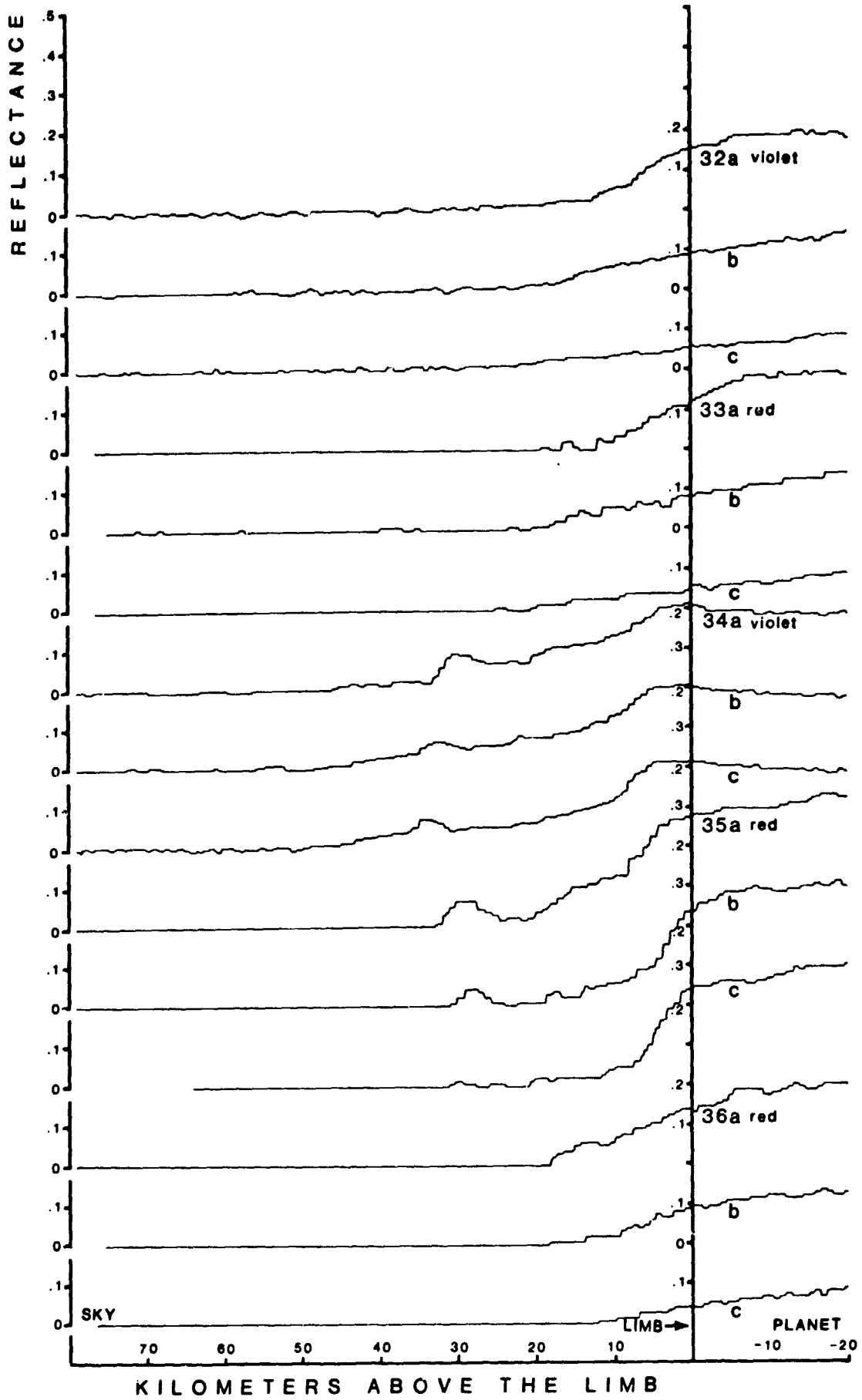

J MARTIN

Figure 21

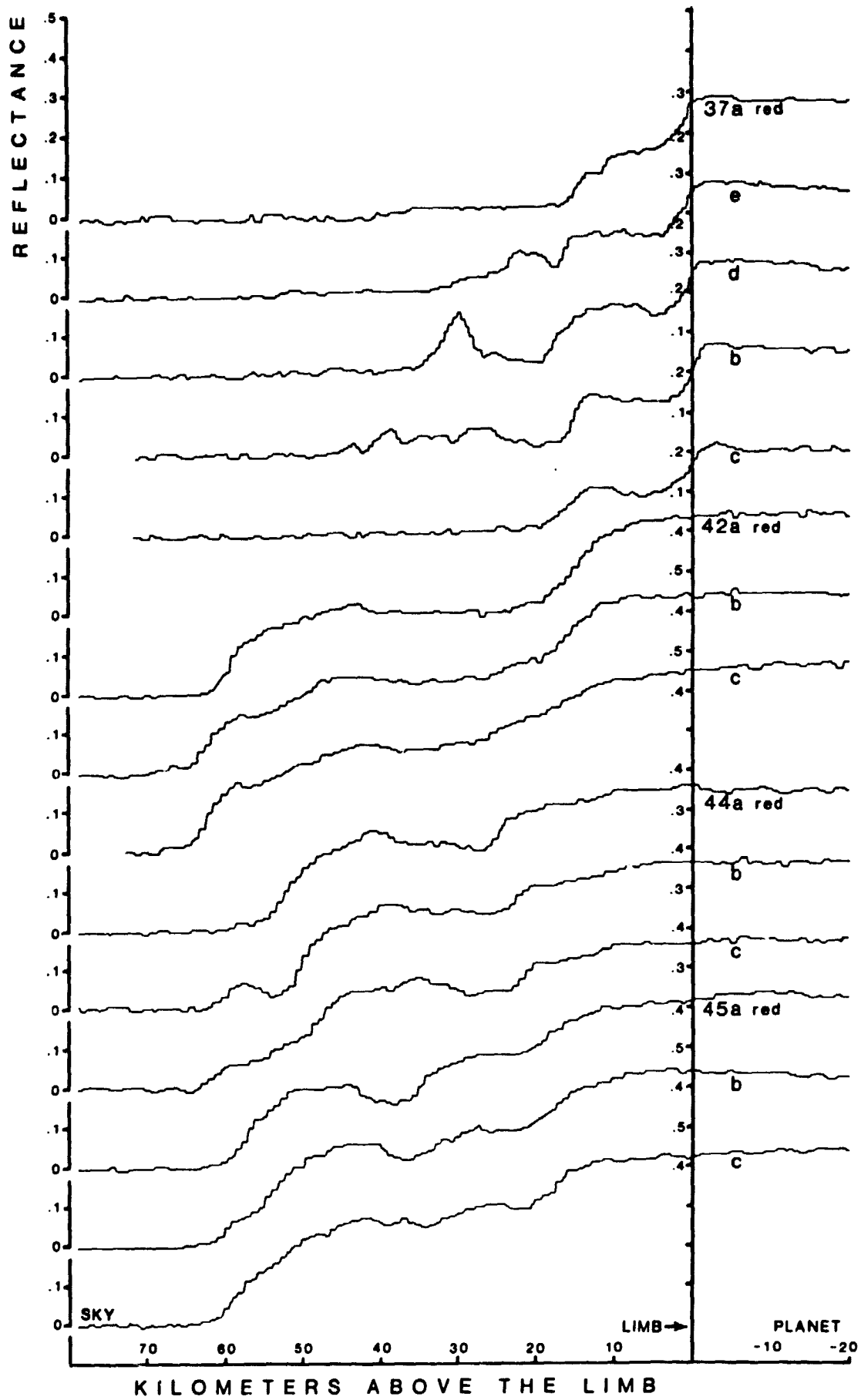

L J MARTIN

Figure 22

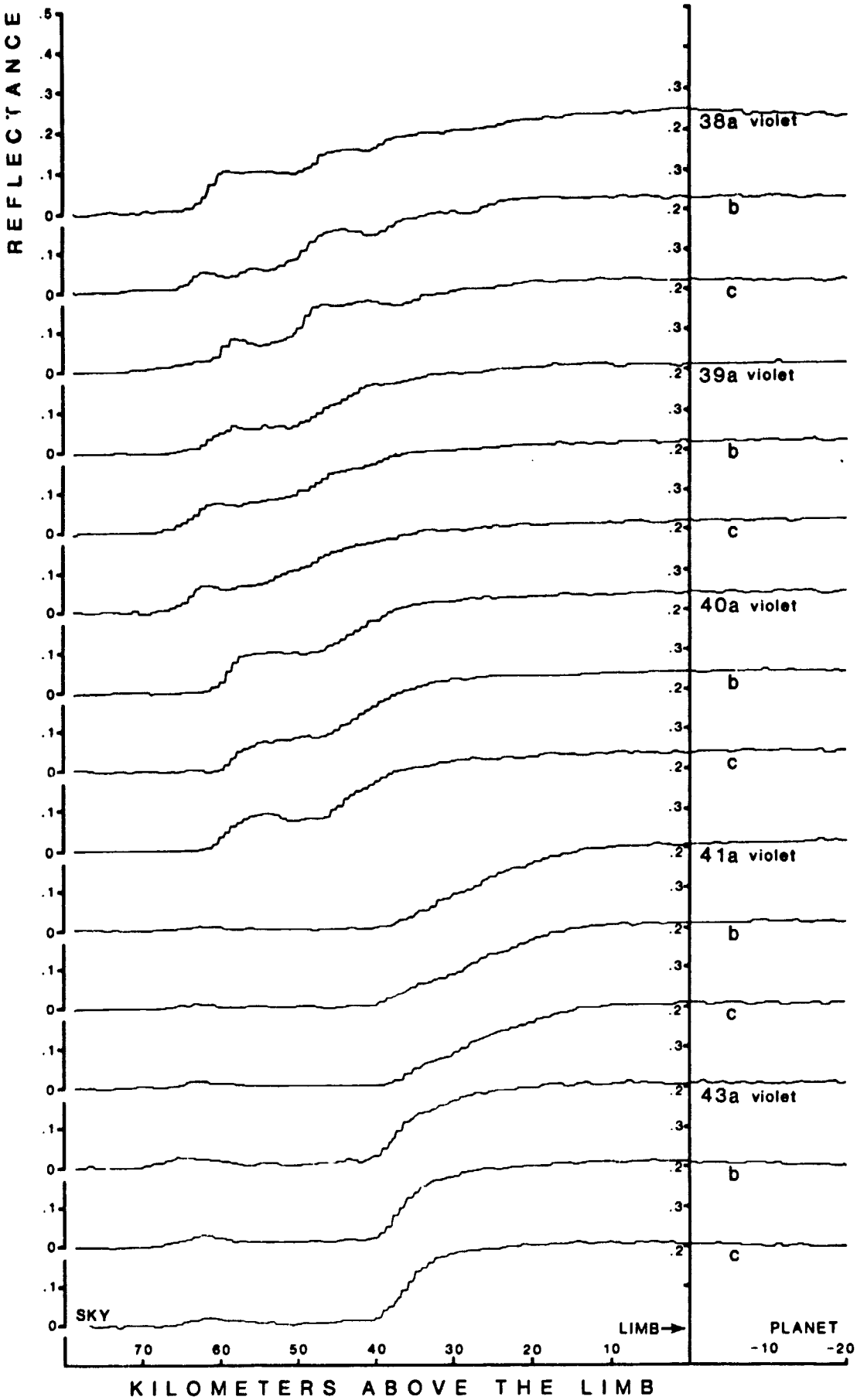

J MARTIN

Figure 23

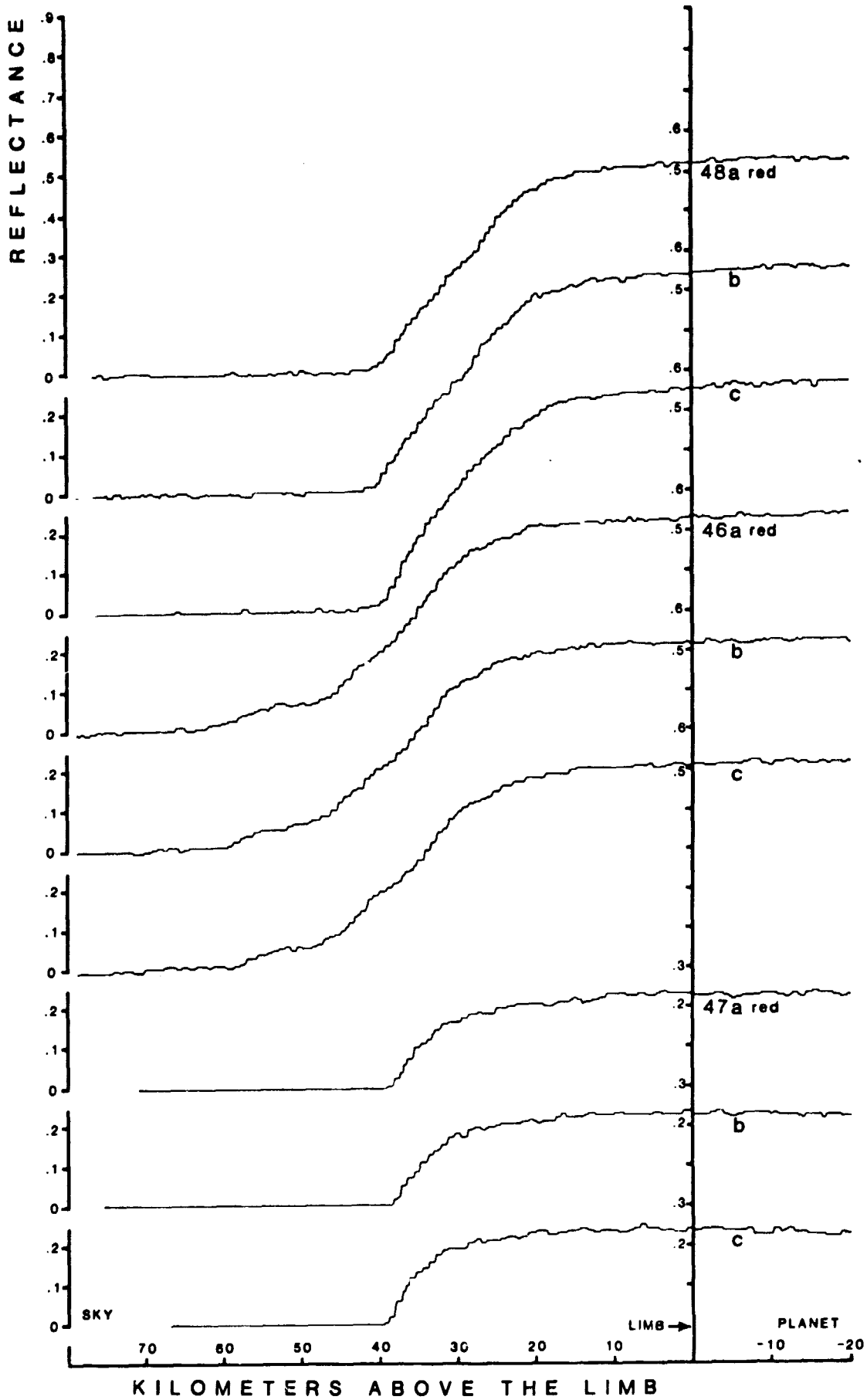

L J MARTIN

Figure 24

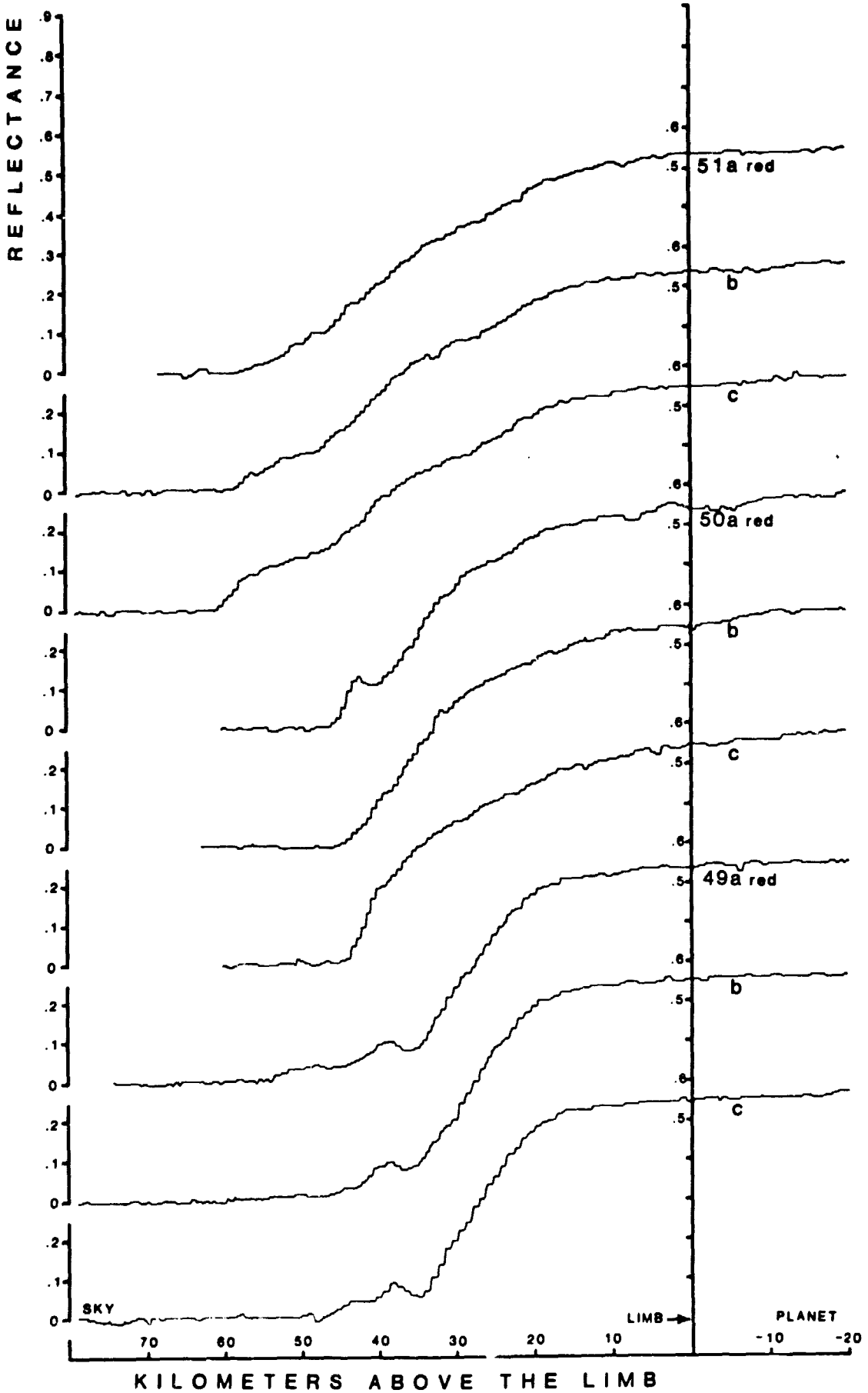

L J MARTIN

Figure 25

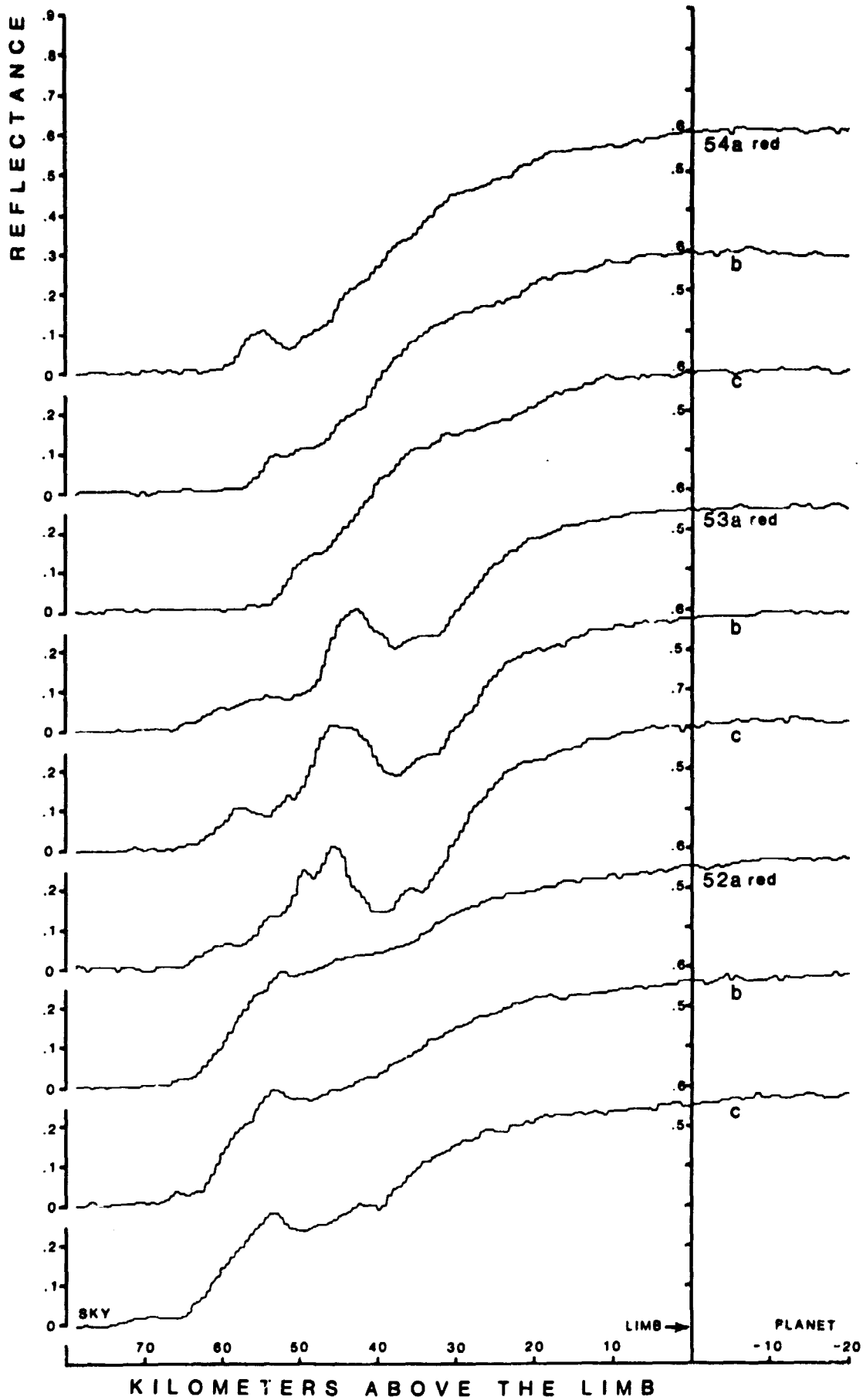

L J MARTIN

Figure 26

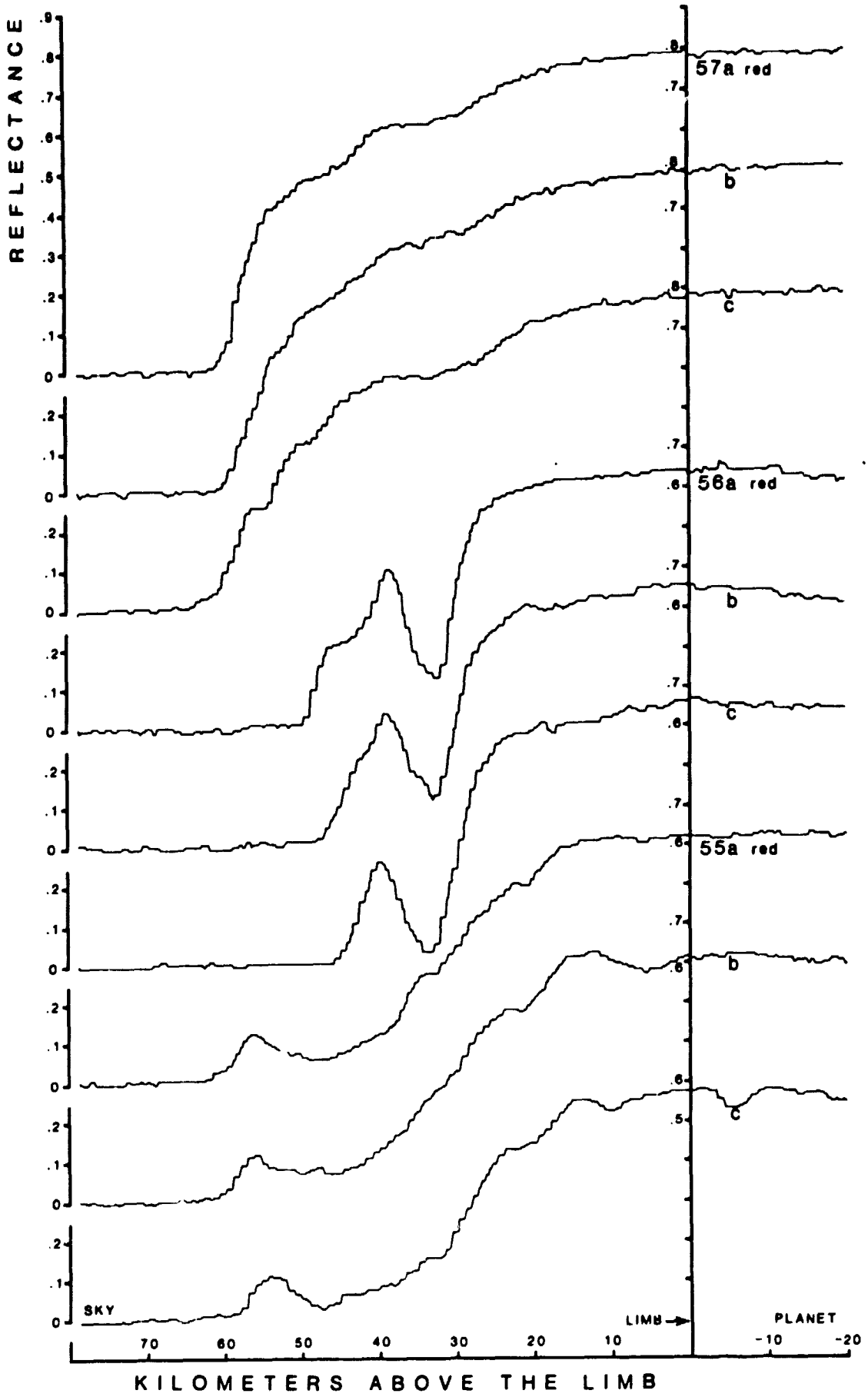

L J MARTIN

Figure 27